

Coupled effect of CNT waviness and agglomeration: A case study of vibrational analysis of CNT/polymer skew plates

Enrique García-Macías^{a,*}, Rafael Castro-Triguero^b

^a*Department of Continuum Mechanics and Structural Analysis, School of Engineering, Universidad de Sevilla, Camino de los Descubrimientos s/n, E-41092-Seville, Spain*

^b*Department of Mechanics, University of Córdoba, Campus de Rabanales, Cordoba, CP 14071, Spain*

Highlights

- A critical comparison of different micromechanics approaches is conducted
- Wavy filler arrangements with agglomeration effects are investigated
- The diagonal symmetry condition and comparison with theoretical bounds are discussed
- Comparison analyses with experimental data are presented
- Coupled effects of waviness and agglomeration are investigated for skew plates

Abstract

The main contribution of this work lies in a critical comparison of different mean-field homogenization approaches for the study of carbon nanotube-reinforced polymers with waviness and agglomeration effects. In particular, this paper focuses on the consistency of predictions in terms of diagonal symmetry of the constitutive tensors and comparison against theoretical bounds. The analysis comprises general axisymmetric orientation distributions of fillers, both planar sinusoidal and helical wavy fillers, as well as different agglomeration schemes by means of a two-parameter agglomeration model. The results demonstrate that waviness and agglomeration simultaneously weaken the macroscopic stiffness of composites. The results also reveal that the widely used Mori-Tanaka method fails to simulate the coupled effect of these two phenomena and, therefore, it is necessary to apply extended approaches with consideration of ad hoc Eshelby's tensors that account for particular wavy microstructures. A case study of carbon nanotube-reinforced skew plates is finally presented to illustrate the coupled effect of waviness and agglomeration on the macroscopic vibrational behavior.

Keywords: Agglomeration, Carbon nanotubes, Diagonal symmetry, Mori-Tanaka method, Skew shells, Waviness

1. Introduction

Over the last decade, numerous publications have reported about the outstanding enhancements of the mechanical properties of polymeric matrices doped with small concentrations of Carbon Nanotubes (CNTs) [1, 2]. Since the mechanical behavior of CNT-reinforced composites is crucially dominated by their microstructure, a reliable dimensioning has to take into consideration their properties as accurately as possible. Three major features are typically distinguished, namely filler statistical orientation distribution, waviness, and agglomeration. Firstly, fillers orientations are governed by complicated flow fields induced by the manufacturing process. Notwithstanding there exists a number of techniques of aligning CNTs (see e.g. [3–5]), most procedures lose effectiveness when embedding the nanotubes throughout the matrix material [6], and, thus, CNTs orientations are typically of statistical nature. Secondly, it has been extensively reported in the literature that due to a high aspect ratio, up to 10^6 [1], as well as a very low bending stiffness, CNTs usually exhibit a certain degree of waviness [7, 8]. Finally, given the electronic configuration of the tube walls and their high specific surface area, CNTs tend to agglomerate and form bundles due to large van de Waals (vdW) attraction forces [9–11]. Although there exists a variety of techniques to improve the dispersion of fillers, including the use of dispersants or sonication, the achievement of

*Corresponding author.

Email address: egarcia28@us.es (Enrique García-Macías)

uniform CNT dispersions is still an intricate task. On the whole, accurate homogenization approaches must allow for considering the coupled effect of waviness and agglomeration.

In order to calculate the effective material properties using microstructural data, several homogenization methods have been proposed in the literature. Since Molecular Dynamics (MD) and multi-scale finite element simulations [12–15] are limited to systems with a small number of atoms due to computational limitations, approaches based on the mean-field homogenization theory have drawn considerable attention. In particular, a large number of recent works in the realm of CNT nanocomposites have been undertaken using the Extended Rule of Mixtures (EROM) [16–18] and the Mori-Tanaka (MT) method [19–21]. The EROM is based upon a modification of the classical Voigt (VT) and Reuss (RS) bounds by the so-called efficiency parameters in order to match the results from a MD or multi-scale simulation [22]. Although many authors have been attracted by the simplicity of this approach, the EROM requires a more sophisticated simulation to tune the efficiency parameters and can only model singular filler configurations. The MT model, on the contrary, allows for the simulation of more complex configurations such as misoriented distribution of fillers, as well as curviness and agglomeration effects [23]. However, although the MT method apparently provides a favorable theoretical framework for the consideration of general arrangements of CNTs, a few research works in the literature report that the MT method may provide diagonally asymmetric stiffness tensors, as well as may violate the Hashin-Shtrikman-Walpole (HSW) bounds [24–27]. In the light of these deficiencies, some authors have sought alternative approaches. Amongst those, it is worth noting the contribution by Ferrari [28], and later extended by Dunn *et al.* [29] (DUN), who proposed to use the strain-concentration tensor given by that of the MT method for perfectly aligned fibers. Another relevant work was the one by Schjødt-Thomsen and Pyrz (STP) [30] who proposed a novel micromechanics approach based upon the direct integration of the MT stiffness tensor for perfectly aligned inclusions. More recently, Zhupanska [31] studied the applicability of the MT method to estimate the elastic moduli of buckypaper doped with Single-Walled CNTs (SWCNTs). In the case of randomly oriented SWCNTs, his results showed that the MT method only provides results comprised between the HSW bounds for moderate filler contents, yielding inadmissible results for high filler concentrations.

All studies agree on the detrimental impact of curviness on the mechanical properties of CNT/polymer nanocomposites. Finite element simulations were proposed by Fisher *et al.* [32] and Bradshaw *et al.* [33] to analyze the planar sinusoidal parametrization of CNTs proposed by Hsiao and Daniel [34]. Another noteworthy contribution was done by Shi *et al.* [23] who extended the MT method for three-dimensional helical CNTs. In that work, their results showed that composites doped with aligned wavy CNTs experience critical reductions in the longitudinal modulus, whilst the lateral moduli slightly increase. Yanase *et al.* [35] proposed an ad hoc Eshelby's tensor (YNS) to account for planar sinusoidal CNTs. In their model, the integration of localized changes in orientation was combined with the MT model to derive closed-form solutions of the effective stiffness. Matveeva *et al.* [36] studied both sinusoidal and helical models by finite element-based homogenization methods, analytical models and MD simulations. It was shown that both geometries significantly reduce the longitudinal elastic stiffness of the composite for fully aligned wavy fillers.

A second important feature of the microstructure is related to the tendency of CNTs to agglomerate in bundles. A noticeable contribution in this respect is the work by Shi *et al.* [23] who introduced a two-parameter agglomeration model. That approach consists of considering agglomerates as ellipsoidal inclusions so that one can conduct the homogenization process in two separate steps. Their results demonstrated substantial decreases in the elastic moduli of composites, what supports the widespread idea of agglomeration as microstructural defects. Although only a few works report about this issue, the two-parameter agglomeration method has been widely accepted. For instance, numerous efforts have been made to study the influence of agglomeration on the mechanical response of CNT-reinforced structural elements (see e.g. [37–40]).

In this study, a critical comparison of different mean-field homogenization approaches for the estimation of the elastic moduli of SWCNT-reinforced polymer composites is presented. For different filler axisymmetric orientation distributions, the suitability of the MT, SC, DUN and STP approaches is assessed in terms of diagonal symmetry and comparison against the HSW and VT/RS bounds. Microstructural features such as CNT volume fraction, aspect ratio, and chirality are also investigated. Afterward, approaches concerning waviness effects, namely the MT, STP and YNS models, are analyzed for both sinusoidal and helical geometries. The influence of CNT agglomeration is studied through the two-parameter agglomeration framework. Most studies limit themselves to the consideration of waviness and agglomeration effects acting independently. However, both phenomena are simultaneously found in practice. The results of this work show that the MT method fails to simulate the coupled effect of these two phenomena, given that its estimates for random filler arrangements are insensitive to waviness. In addition, it is evidenced that the MT predictions for composites doped with fully aligned wavy CNTs are highly asymmetric. By considering the combination of the YNS approach and the two-parameter agglomeration model, it is noted that the weakening effects of waviness and agglomeration add up when acting simultaneously. In addition, comparison analyses with experimental data are presented to illustrate the importance of the coupled

Table 1: Abbreviations used throughout the present paper for proper handling.

DE	Dilute Eshelby
MT	Mori-Tanaka
SC	Self-consistent
STP	Schjødt-Thomsen and Pyrz
DUN	Dunn
YNS	Yanase
L-HSW	Hashin-Shtrikman-Walpole lower bound
U-HSW	Hashin-Shtrikman-Walpole upper bound
RS	Reuss bound
VT	Voigt bound

effect of waviness and agglomeration for moderate filler contents. Finally, a case study is also presented to illustrate the coupled weakening effect of filler waviness and agglomeration on the macroscopic dynamic behavior of CNT-reinforced skew plates.

The remainder of this paper is organized as follows: Section 2 concisely presents the micromechanics approaches used in this research work. Section 3 presents the used approaches for analyzing the waviness effects, both for planar sinusoidal and helical geometries. Section 4 describes the basis of the two-parameter agglomeration model. Finally, Section 5 includes the numerical results and discussion, and Section 6 concludes the paper.

Throughout the paper, a boldface letter stands for a fourth-order tensor, $\mathbf{A} \equiv A_{ijkl}$, and a colon between two tensors denotes inner product, $\mathbf{A} : \mathbf{B} \equiv A_{ijkl}B_{klmn}$

Abbreviations. To distinguish the regarded methods, several abbreviations have been introduced as a reference for readership in Table 1.

2. Mean-field micromechanics modeling

2.1. Fundamentals of effective medium theory

Let V denote the Representative Volume Element (RVE) of a polymer matrix doped with a sufficient number of CNTs in such a way that the overall properties of the composite are statistically represented [41]. It is assumed that CNTs are transversely isotropic inclusions dispersed according to an arbitrary Orientation Distribution Function (ODF). The matrix is defined as isotropic and perfect bonding between phases is assumed. In accordance with the notation of Hill [42] and Walpole [43], the tensor of elastic moduli of CNTs, \mathbf{C}_f , can be noted as $\mathbf{C}_f = (2k_r, l_r, n_r, 2m_r, 2p_r)$, where k_r , l_r , m_r , n_r and p_r are fiber Hill's elastic moduli; k_r is the plane-strain bulk modulus normal to the fiber direction, n_r is the uniaxial tension modulus in the fiber direction, l_r is the associated cross modulus, m_r and p_r are the shear moduli in planes normal and parallel to the fiber direction, respectively. Similarly, the matrix phase can be noted as $\mathbf{C}_m = (3\kappa_m, 2\mu_m)$, with κ_m and μ_m being the matrix's bulk and shear moduli, respectively. In conjunction with the used notations, the constitutive matrix for inclusions with transversely isotropic properties (with x'_1 - x'_3 as the isotropy plane) takes the form:

$$\mathbf{C}_f = \begin{bmatrix} k_r + m_r & l_r & k_r - m_r & 0 & 0 & 0 \\ l_r & n_r & l_r & 0 & 0 & 0 \\ k_r - m_r & l_r & k_r + m_r & 0 & 0 & 0 \\ 0 & 0 & 0 & p_r & 0 & 0 \\ 0 & 0 & 0 & 0 & m_r & 0 \\ 0 & 0 & 0 & 0 & 0 & p_r \end{bmatrix} \quad (1)$$

In order to describe the filler orientations, a reference local coordinate system $\mathbf{K}'' \equiv \{0; x'_1 x'_2 x'_3\}$ is fixed in each fiber. In this paper, it is assumed that all the inclusions are equal and defined as ellipsoids with aspect ratios $a_1 = a_3 < a_2$, being the semi-major axis aligned in the local x'_2 -axis. In general, three Euler angles, θ , γ and ψ , are required to describe the orientation of any orthogonal coordinate system with respect to the global one, $\mathbf{K} \equiv \{0; x_1 x_2 x_3\}$. However, since x'_2 -axis is parallel to the axis of rotational symmetry of the ellipsoids, a rotation around this axis produces no change and ψ can be thus chosen arbitrarily, e.g. $\psi=0$. The resultant configuration is shown in Fig. 1, where the polar and azimuthal angles, θ and γ , are defined by:

$$\theta \equiv \widehat{x_1 x'_1}, \quad \gamma \equiv \widehat{x'_3 x'_2} \quad (2)$$

The base vectors \mathbf{e}_i and \mathbf{e}'_i of the global and local coordinate systems are related via the transformation matrix \mathbf{g} as $\mathbf{e}'_i = g_{ij}\mathbf{e}_j$. The transformation matrix \mathbf{g} is defined by the successive rotations around x_2 and x_1 axes, $\mathbf{R}_1(\gamma)$ and $\mathbf{R}_2(\theta)$, as:

$$\mathbf{g} = \mathbf{R}_1(\gamma)\mathbf{R}_2(\theta) = \begin{bmatrix} \cos(\gamma) & 0 & \sin(\gamma) \\ -\sin\theta\sin(\gamma) & \cos(\theta) & \cos(\gamma)\sin\theta \\ -\cos(\theta)\sin(\gamma) & -\sin\theta & \cos(\theta)\cos(\gamma) \end{bmatrix} \quad (3)$$

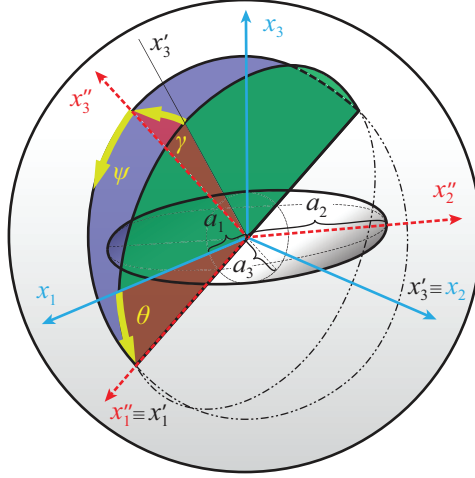


Figure 1: Euler angles defining the relation between the orientation of an ellipsoidal inclusion with an aspect ratio $a_1 = a_3 < a_2$ in the local coordinate system, $\{0; x'_1, x'_2, x'_3\}$ and the global coordinate system, $\{0; x_1, x_2, x_3\}$.

The coordinate transformation of a tensor \mathbf{P} into the local coordinate system \mathbf{K}'' is explicitly represented in terms of the transformation matrix as $P''_{ijkl} = g_{ip}g_{jq}g_{kr}g_{ls}P_{pqrs}$. Due to the high number of inclusions contained in the RVE, the description of their orientation field is of statistical nature. The probability of a filler lying in an infinitesimal range of angles $[\theta, \theta + d\theta] \times [\gamma, \gamma + d\gamma]$ is given by $\Omega(\theta, \gamma) \sin\theta d\theta d\gamma$, with $\Omega(\theta, \gamma)$ being the ODF. The integration of any ODF weighted function $F(\theta, \gamma)$ over all possible orientations in the Euler space, also referred to as the orientational average of F , $\langle F \rangle$, is defined through:

$$\langle F \rangle = \int_0^{2\pi} \int_0^{\pi/2} F(\theta, \gamma) \Omega(\theta, \gamma) \sin\theta d\theta d\gamma \quad (4)$$

Throughout this work, indexes “ f ” and “ m ” refer the corresponding quantity to the portions of V occupied by the inclusions and the matrix, respectively. Moreover, the volume fractions occupied by the inclusions and the matrix are denoted as f_f and $f_m = 1 - f_f$, respectively. In addition, the relationship between the average strain in the inclusions and in the matrix phase is governed by the strain concentration tensor \mathbf{A} as [41]:

$$\bar{\boldsymbol{\epsilon}}^f = \mathbf{A} : \bar{\boldsymbol{\epsilon}}^m \quad (5)$$

Let us note that the tensor \mathbf{A} is not necessarily diagonally symmetric, $A_{ijkl} \neq A_{klij}$, although minor symmetry is always guaranteed, that is $A_{ijkl} = A_{jikl} = A_{ijlk}$. The rule of mixtures between the strain and stress tensors of the constituent phases, and (5), along with the elastic constitutive laws for both phases, that is $\bar{\boldsymbol{\sigma}}^f = \mathbf{C}_f : \bar{\boldsymbol{\epsilon}}^f$ and $\bar{\boldsymbol{\sigma}}^m = \mathbf{C}_m : \bar{\boldsymbol{\epsilon}}^m$, suffice to identify the effective stiffness tensor \mathbf{C} as [30]:

$$\mathbf{C} = \mathbf{C}_m + f_f \langle (\mathbf{C}_f - \mathbf{C}_m) : \mathbf{A} \rangle \quad (6)$$

Different assumptions on the tensor \mathbf{A} correspond to different effective medium theories.

2.2. Mori-Tanaka approach

The Mori-Tanaka (MT) method [44] extends the theory of Eshelby [45, 46], restricted to one single inclusion embedded in an isotropic semi-infinite medium, to the case of a finite domain doped with multiple inhomogeneities. The Eshelby’s equivalent inclusion method (DE) demonstrated that the strain concentration tensor for the limit case of a single anisotropic ellipsoidal inhomogeneity in an infinite matrix, \mathbf{A}^{dil} , reads:

$$\mathbf{A}^{\text{dil}} = [\mathbf{I} + \mathbf{S} : \mathbf{C}_m^{-1} : (\mathbf{C}_f - \mathbf{C}_m)]^{-1} \quad (7)$$

where \mathbf{I} is the identity tensor, and \mathbf{S} is the Eshelby’s tensor, well documented in [45, 47]. Then, at non-dilute filler concentrations, Mori and Tanaka proposed the combination of the equivalent elastic inclusion idea of Eshelby,

and an interaction between particles to be given by the concept of average stress in the matrix. According to Benveniste's revision [48], the strain concentration tensor \mathbf{A}^{MT} provided by the MT method writes:

$$\mathbf{A}^{\text{MT}} = \mathbf{A}^{\text{dil}} : \left[(1 - f_r)\mathbf{I} + f_r \langle \mathbf{A}^{\text{dil}} \rangle \right]^{-1} \quad (8)$$

2.3. Self-consistent effective-medium approach

At high concentrations of inhomogeneities, the far-field interaction hypothesis of the MT method becomes uncertain. Typically, an alternative strategy for obtaining mean-field estimates of the properties of non-dilute inhomogeneous materials is the Self-Consistent (SC) method. In this case, the interaction between phases is approximated by assuming that inclusions are embedded in an effective medium with yet unknown elastic tensor \mathbf{C}^* . Hence, the SC estimates of the effective stiffness tensor write [42]:

$$\mathbf{C}^{\text{SC}} = \mathbf{C}^* + f_r \langle (\mathbf{C}_f - \mathbf{C}^*) : \mathbf{A}^{\text{SC}} \rangle \quad (9)$$

where \mathbf{A}^{SC} reads:

$$\mathbf{A}^{\text{SC}} = \left[\mathbf{I} + \mathbf{S}^* (\mathbf{C}^*)^{-1} : (\mathbf{C}_r - \mathbf{C}^*) \right]^{-1} \quad (10)$$

Since \mathbf{C}^* is not known a priori, the SC scheme is an implicit method and must be solved in an iterative way. An additional change is that the Eshelby's tensor \mathbf{S}^* is not a function of the matrix stiffness, \mathbf{C}_m , but of the effective stiffness tensor, \mathbf{C}^* , which is transversely isotropic. Expressions of the Eshelby's tensor for an ellipsoid of revolution in a transversely isotropic medium were given by Chou *et al.* [49] and by Lin and Mura [50].

2.4. Extended Mori-Tanaka approaches

As previously discussed, a few research works in the literature report that the MT method may provide diagonally asymmetric stiffness tensors, as well as may violate the HSW bounds [24–27]. Note that the effective stiffness tensor \mathbf{C}^{MT} is diagonally symmetric if and only if so is the second term on the right side of Eq. (6) for non-vanishing values of f_r . Nonetheless, this condition is not usually fulfilled for general two-phase composites, what results in physically unacceptable stiffness tensors. Therefore, the use of the MT model is only justified in cases where symmetry is guaranteed such as [26]: (i) random orientation distribution of inclusions, (ii) perfect alignment of inclusions, (iii) isotropic inclusions, or (iv) spherical inclusions. A second flaw of the MT method concerns its questionable predictions at high filler concentrations. In particular, the resulting \mathbf{C}^{MT} from Eqs. (6) and (8) depends on the matrix moduli for f_r approaching 1. In view of these limitations, some authors have proposed alternative approaches. In this paper, the extended MT approaches proposed by Dunn *et al.* [29] and Schjødt-Thomsen and Pyrz [30] are compared.

2.4.1. Dunn approach

Following the studies of Ferrari [28], Dunn *et al.* [29] proposed to use the strain-concentration tensor given by the MT concentration tensor for perfectly aligned fillers as follows:

$$\mathbf{A}^{\text{DUN}} = \mathbf{A}^{\text{dil}} : \left[(1 - f_r)\mathbf{I} + f_r \mathbf{A}^{\text{dil}} \right]^{-1} \quad (11)$$

thus, the stiffness tensor for two-phase composites with inclusions of identical shape reads:

$$\mathbf{C}^{\text{DUN}} = \mathbf{C}_m + f_r \left[\langle \mathbf{C}_f \mathbf{A}^{\text{DUN}} \rangle - (1 - f_r) \langle \mathbf{A}^{\text{DUN}} \rangle \right] \quad (12)$$

2.4.2. Schjødt-Thomsen and Pyrz approach

Another prominent alternative is the one proposed by Schjødt-Thomsen and Pyrz (STP) [30]. This approach utilizes a direct integration of the MT stiffness tensor for the case of perfectly aligned fillers with respect to the ODF as:

$$\mathbf{C}^{\text{STP}} = \int_0^{2\pi} \int_0^{\pi/2} \mathbf{C}(\theta, \gamma) \Omega(\theta, \gamma) \sin \theta d\theta d\gamma \quad (13)$$

with $C(\theta, \gamma)_{ijkl} = g_{ip} g_{jq} g_{kr} g_{ls} C(0, 0)_{pqrs}^{\text{MT}}$.

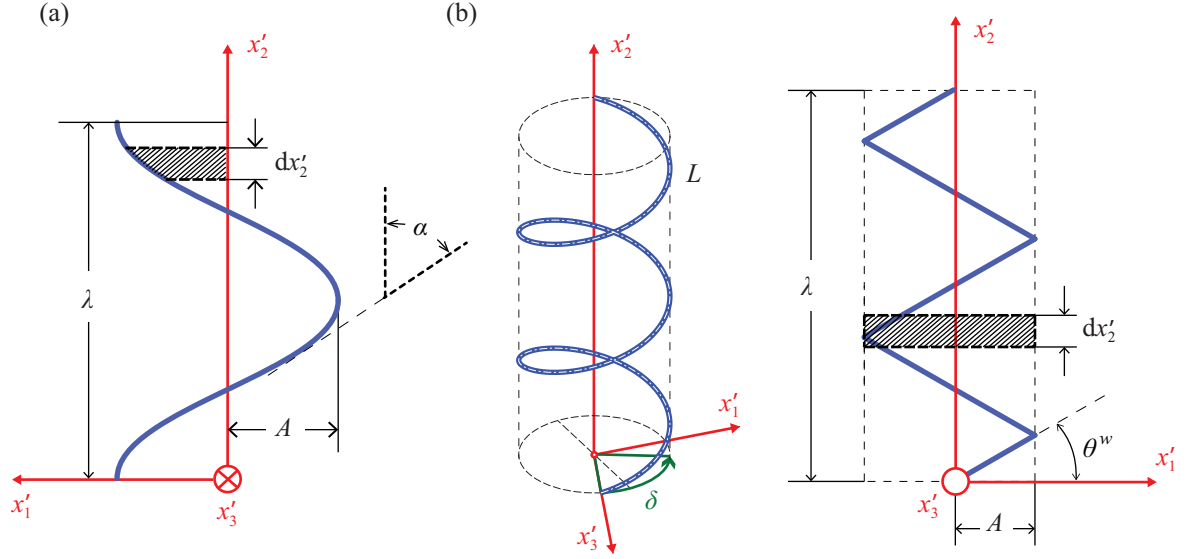


Figure 2: Planar sinusoidal (a) and helical model (b) of a curved CNT.

3. Modeling of CNT waviness

In order to characterize the wavy state of CNTs, different curved geometries have been proposed in the literature such as planar sinusoidal curves [32, 34], helices [23, 51], and polylines with straight segments [52]. In this work, planar sinusoidal and helical geometries, as sketched in Figs. 2 (a) and (b), respectively, are studied. In order to compute the overall properties of CNT/polymer composites with waviness effects, three different homogenization approaches are compared, namely the MT method, the extension of the STP approach for wavy CNTs, and the YNS approach.

3.1. Planar sinusoidal nanotubes

The planar sinusoidal approach in Fig. 2 (a) is defined in the $x'_1 - x'_2$ plane by its amplitude, A , and wave length, λ , as:

$$x'_3 = 0, \quad x'_2 = x'_2, \quad x'_1 = A \cos \frac{2\pi x'_2}{\lambda} \quad x'_2 \in [0, \lambda] \quad (14)$$

3.1.1. Mori-Tanaka approach

The application of the MT framework to the study of wavy CNT-reinforced composites was first conducted by Shi *et al.* [23] for the analysis of helical nanotubes. The main hypothesis of this approach is that, when the filler wavelength becomes far larger than its amplitude, the average strain in the filler section approaches that of an infinitely long straight fiber. Hence, the average strain at every differential slice, dx'_2 , can be estimated as that of an infinitely long straight fiber oriented at an angle $\alpha(x'_2)$. On this basis, the approach proposed by Shi *et al.* [23] can be extended to planar sinusoidal CNTs as follows:

$$\mathbf{C}^{\text{MT}} = \left[\frac{f_r}{V_c} \int_0^\lambda (\mathbf{C}_r(x'_2) : \mathbf{A}(\alpha(x'_2), 0) : \mathbf{C}_m^{-1}) dV_c + f_m \mathbf{I} \right] : \left[\frac{f_r}{V_c} \int_0^\lambda (\mathbf{A}(\alpha(x'_2), 0) : \mathbf{C}_m^{-1}) dV_c + f_m \mathbf{C}_m^{-1} \right]^{-1} \quad (15)$$

with V_c being the volume of a CNT given by:

$$V_c = \frac{\pi d_c^2}{4} \int_0^\lambda \frac{dx'_2}{\cos \alpha(x'_2)} = \frac{\pi d_c^2}{4} I_v \quad (16)$$

where d_c is the diameter of the CNTs. The angle $\alpha(x'_2)$ in Eq. (15) can be obtained by differentiating Eq. (14), what yields:

$$\alpha(x'_2) = \tan^{-1} \left[\frac{dx'_1}{dx'_2} \right] = \tan^{-1} \left[-\frac{2\pi A}{\lambda} \sin \left(\frac{2\pi x'_2}{\lambda} \right) \right] \quad (17)$$

3.1.2. Schjødt-Thomsen and Pyrz approach

The direct integration of the STP approach can be also applied in this context integrating the stiffness tensor along the curved trace as:

$$\mathbf{C}^{\text{STP}} = \frac{1}{I_v} \int_0^\lambda \frac{\mathbf{C}(\alpha(x'_2), 0)}{\cos \alpha(x'_2)} dx'_2 \quad (18)$$

being $\mathbf{C}(\alpha(x'_2), 0)$ the MT estimate for straight fibers with polar angle $\alpha(x'_2)$ given in Eq. (17).

3.1.3. Ad hoc Eshelby's tensor approach

An ad hoc Eshelby's tensor to account for waviness effects was proposed by Yanase (YNS) *et al.* [35]. According to this model, the effective stiffness of wavy CNT-reinforced composites is evaluated by the following integral:

$$\bar{\mathbf{C}} = \frac{1}{I_v} \int_0^\lambda \frac{\mathbf{C}^*(\alpha(x'_2), 0)}{\cos \alpha(x'_2)} dx'_2 \quad (19)$$

with \mathbf{C}^* being the solution of the Eshelby's equivalent problem as:

$$\mathbf{C}^* = \mathbf{C}_m + f_r (\mathbf{C}_f - \mathbf{C}_m) : \mathbf{A}^{\text{dil}} \quad (20)$$

In order to reproduce Eq. (19) with the Eshelby's equivalent inclusion method, an ad hoc Eshelby's tensor, $\bar{\mathbf{S}}$, can be evaluated as follows:

$$\bar{\mathbf{S}} = \lim_{f_r \rightarrow 0} \left[f_r \left((\mathbf{C}_m)^{-1} : \bar{\mathbf{C}} - \mathbf{I} \right)^{-1} - (\mathbf{C}_f - \mathbf{C}_m)^{-1} : \mathbf{C}_m \right] \quad (21)$$

where the limit is taken to exclude the far-field interaction. Moreover, if the wavy fibers are randomly oriented, the ad hoc Eshelby's tensor of Eq. (21) can be integrated around the alignment axis, x'_2 :

$$\mathbf{S}^* = \frac{1}{2\pi} \int_0^{2\pi} \bar{\mathbf{S}}(0, \gamma) d\gamma \quad (22)$$

Now, the effective stiffness of wavy CNT-reinforced composites at non-dilute regimes can be computed on the basis of the MT assumption considering the following dilute strain concentration tensor:

$$\mathbf{A}^{\text{dil, YNS}} = \left[\mathbf{I} + \mathbf{S}^* : \mathbf{C}_m^{-1} : (\mathbf{C}_f - \mathbf{C}_m) \right]^{-1} \quad (23)$$

3.2. Helical nanotubes

The helical curve is parametrized by its radius, A , spiral angle, θ^w , and polar angle, δ , as:

$$x'_1 = A \sin \delta, \quad x'_2 = x'_2, \quad x'_3 = A \cos \delta \quad x'_2 \in [0, \lambda] \quad (24)$$

where the wave length can be expressed as $\lambda = L \sin \theta^w$, being $L = \delta A / \cos \theta^w$ the length of the curve. The spiral angle θ^w ranges from 0 to $\pi/2$ and governs the curvature of the filler. For instance, $\theta^w = \pi/2$ corresponds to a straight CNT, while $\theta^w = 0$ corresponds to a circular CNT.

3.2.1. Mori-Tanaka approach

In this case, the helical approach was developed by Shi *et al.* [23] as:

$$\mathbf{C}^{\text{MT}} = \left[\frac{f_r}{\delta} \int_0^\delta (\mathbf{C}_r(\theta^w, s) : \mathbf{A}(\theta^w, s) : \mathbf{C}_m^{-1}) ds + f_m \mathbf{I} \right] : \left[\frac{f_r}{\delta} \int_0^\delta (\mathbf{A}(\theta^w, s) : \mathbf{C}_m^{-1}) ds + f_m \mathbf{C}_m^{-1} \right]^{-1} \quad (25)$$

3.2.2. Schjødt-Thomsen and Pyrz approach

In a similar way to planar sinusoidal configurations, the STP approach can be also applied to helical nanotubes as follows:

$$\mathbf{C}^{\text{STP}} = \frac{1}{\delta} \int_0^\delta \mathbf{C}(\theta^w, \gamma) d\gamma \quad (26)$$

being in this case $\mathbf{C}(\theta^w, s)$ the MT estimate for straight fillers with constant polar angle θ^w and azimuthal angle γ varying from 0 to δ .

3.2.3. Ad hoc Eshelby's tensor approach

Finally, the YNS approach can be extended to helical geometries as:

$$\bar{\mathbf{C}} = \frac{1}{\delta} \int_0^\delta \mathbf{C}^*(\theta^w, \gamma) d\gamma \quad (27)$$

with \mathbf{C}^* being the Eshelby's equivalent inclusion solution given in Eq. (20). In this case, helical wavy nanotubes affect both transverse directions and, thus, the integral in Eq. (22) is not required to model random orientations of CNTs. Hence, Eq. (23) can be directly used considering $\mathbf{S}^* = \bar{\mathbf{S}}$.

4. Modeling of CNT agglomeration

In this paper, the two-parameter agglomeration model introduced by Shi *et al.* [23] is adopted to estimate the effective mechanical properties of heterogeneous dispersions of CNTs. This approach differentiates two regions, one with high filler concentration, corresponding to clusters, and another with low filler concentration, i.e. the surrounding composite. Hence, the total volume of CNTs, V_r , dispersed in V , can be divided into the following two parts:

$$V_r = V_r^{bundles} + V_r^m \quad (28)$$

where $V_r^{bundles}$ and V_r^m denote the volumes of CNTs dispersed in the bundles and in the surrounding matrix, respectively. In order to characterize the agglomeration of CNTs in bundles, two parameters, ξ and ζ , are introduced as follows:

$$\xi = \frac{V_{bundles}}{V}, \quad \zeta = \frac{V_r^{bundles}}{V_r} \quad (29)$$

where $V_{bundles}$ is the volume occupied by the bundles in the RVE. The agglomeration parameter ξ represents the volume ratio of bundles with respect to the total volume of the RVE. On the other hand, ζ stands for the volume ratio of CNTs within the bundles with respect to the total volume of fillers. This pair of parameters unequivocally defines the agglomeration scheme as outlined in Fig. 3. After some manipulations, the CNT volume fractions in the bundles and the surrounding composite, c_1 and c_2 , respectively, can be expressed as:

$$c_1 = f_r \frac{\zeta}{\xi}, \quad c_2 = f_r \frac{1 - \zeta}{1 - \xi} \quad (30)$$

It is extracted from Eq. (30) that $\zeta \geq \xi$ must be fulfilled in order to impose a higher filler concentration in the clusters. The limit case $\zeta = \xi$ represents an uniform distribution of fillers, whilst the heterogeneity degree grows for larger values of ζ up to $\zeta = \min(1, \xi/f_r)$. Hence, the homogenization process takes place in two separate steps. Firstly, the overall constitutive tensors of the bundles, \mathbf{C}^{in} , and the surrounding composite, \mathbf{C}^{out} , are obtained with polymer as matrix and CNTs as inclusions with volume fractions c_1 and c_2 , respectively. Secondly, the overall constitutive tensor of the composite, \mathbf{C}^* , is computed considering the surrounding composite as matrix and bundles as inclusions. On this basis, whichever of the previously presented micromechanics models can be extended to account for agglomeration effects.

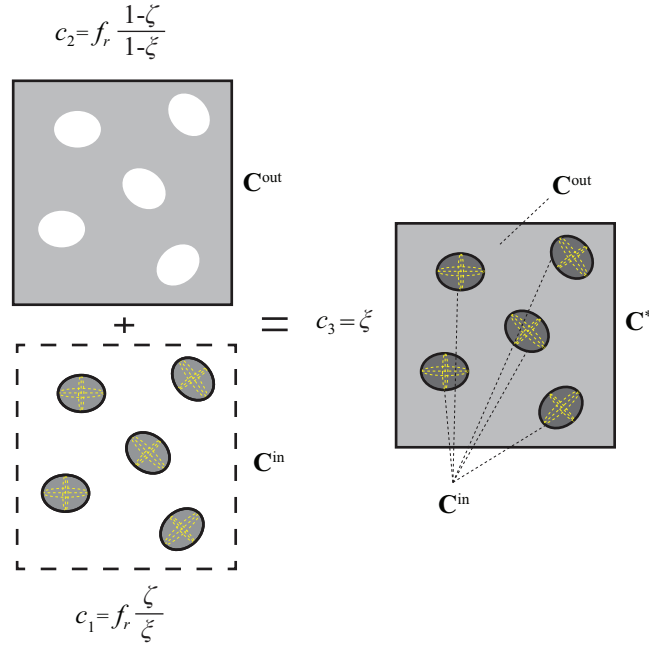


Figure 3: Schematic representation of the two parameter agglomeration model.

5. Results and discussion

In this section, numerical simulations are conducted in order to compare the previously introduced approaches for different CNTs configurations. The discussion particularly focuses on the diagonal symmetry consistency and the comparison with reference bounds, including the Voigt/Reuss (VR) and Hashin-Shtrikman-Walpole (HSW) bounds. Case studies evaluate uniform filler dispersions, effects of non-straightness and agglomeration. For illustrative purposes, the polymer matrix is selected as a thermosetting polymer Epon 862/EPI cure W with elastic properties $E_m=2.55$ GPa and $\nu_m=0.2$ [31]. As reinforcing phase, different SWCNTs are studied with Hill's elastic moduli included in Table 2. Details on the definition of the Hill's elastic moduli in terms of engineering constants can be found in reference [53]. The discussion is organized into five cases: Subsection 5.1 presents a discussion on polymers doped with well dispersed straight CNTs, Subsection 5.2 studies the different approaches for accounting for wavy CNTs, Subsection 5.3 discusses the effects of agglomeration of CNTs in bundles, Subsection 5.4 analyzes the coupled effect of waviness and agglomeration and, finally, Subsection 5.5 furnishes comparison analyses against experimental data. It must be indicated that, in practice, CNT volume fractions are typically below 10%. Higher volume fractions result in excessive filler agglomerations and the theoretical approaches provide unrealistic estimates as it is shown below in Subsection 5.5. However, in the subsequent analyses, filler volume fractions up to 100% are presented for illustrative purposes. A case study of free vibration of CNT-reinforced skew plates in Subsection 5.6 closes this section as a full-scale application example.

Table 2: Hill's elastic moduli for several armchair Single-Walled Carbon Nanotubes (SWCNTs) [19, 54].

CNT	k_r [GPa]	l_r [GPa]	m_r [GPa]	n_r [GPa]	p_r [GPa]
SWCNT (5,5)	536	184	132	2143	791
SWCNT (10,10)	271	88	17	1089	442
SWCNT (15,15)	181	58	5	726	301
SWCNT (20,20)	136	43	2	545	227
SWCNT (50,50)	55	17	0.1	218	92

5.1. Polymer doped with well dispersed straight CNTs

First, uniform dispersions of straight CNTs are studied, including fully aligned and misoriented fillers arrangements are analyzed, as well as microstructural features such as CNT volume fraction, aspect ratio, and chirality.

5.1.1. Uniaxially aligned CNTs

In this first set of analyses, uniform dispersions of uniaxially aligned straight CNTs are studied. Traditionally, bounds on elastic properties of composites are utilized for assessing the validity of homogenization approaches.

In this paper, the Voigt (VT) [55] and Reuss (RS) bounds [56], as well as the Hashin-Shtrikman-Walpole (HSW) bounds [57–59] have been considered. Figure 4 shows the effective elastic moduli of polymer composites reinforced by aligned straight SWCNTs (10,10). The longitudinal, E_{\parallel} , and transverse elastic moduli, E_{\perp} , are depicted against the filler volume fraction f_r , whose expressions can be related to the Hill’s elastic moduli as:

$$E_{\parallel} = n - \frac{l^2}{k}, \quad E_{\perp} = \frac{4m(kn - l^2)}{kn - l^2 + mn} \quad (31)$$

The previously outlined homogenization approaches are compared, namely the MT, DE, and SC approaches, as well as the RS/VT and HSM bounds. Let us recall that, in the case of fully aligned inclusions, all the analyzed approaches are well-known to provide diagonally symmetric estimates. For this reason, diagonal symmetry verifications are obviated in this test. It is noted that CNTs are highly anisotropic, with longitudinal Young’s moduli two orders of magnitude higher than the transverse ones. Accordingly, it is observed in Fig. 4 that E_{\parallel} increases much more rapidly with the volume fraction f_r than E_{\perp} . Very little differences are found in E_{\parallel} among the different approaches in Fig. 4 (a). Conversely, larger differences arise for E_{\perp} in Fig. 4 (b), especially for filler contents above 0.4. The DE approach ignores any interaction between particles so it is only valid for low filler volume fractions (asymptotically correct to $\mathcal{O}(f_r)$). With regard to the SC scheme, it exhibits a typical behavior approximating the HSW bounds at low and high volume fractions, and displays a transition sigmoid curve in-between. For instance, at filler content $f_r=0.8$, the MT model predicts a transverse Young’s modulus of 15 GPa, while the SC approach yields a value of 52.11 GPa, almost four times the former.

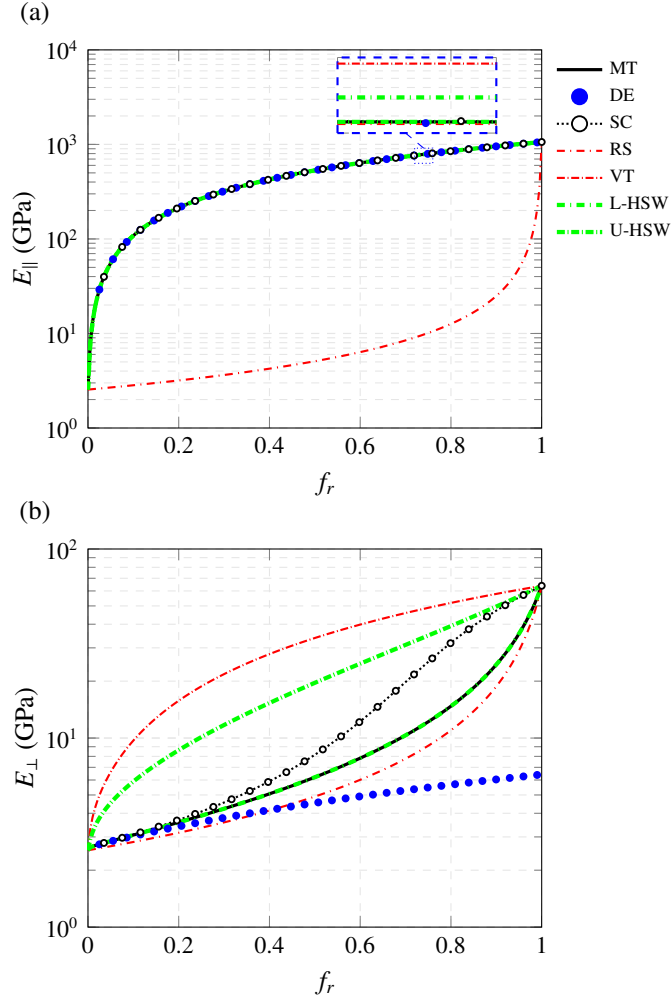


Figure 4: Effective Young’s modulus in the longitudinal direction E_{\parallel} (a) and in the transverse direction E_{\perp} (b) versus filler volume fraction f_r of Epon 862/EPI cure W reinforced by aligned, infinitely long straight SWCNTs (10,10).

The longitudinal Young’s modulus of nanocomposites with different CNT aspect ratios (a_1, a_2, a_3) is shown in Fig. 5. In particular, fillers range from spherical particles, (1,1,1), to infinitely long fibers, (1, ∞ ,1). The effective

properties have been estimated by the MT method and the SC approach, corresponding to solid and dotted lines, respectively. It can be seen that E_{\parallel} increases with increasing CNT lengths. Also, it is observed that the estimates by both the MT and SC approaches get proximate as the CNT aspect ratio increases.

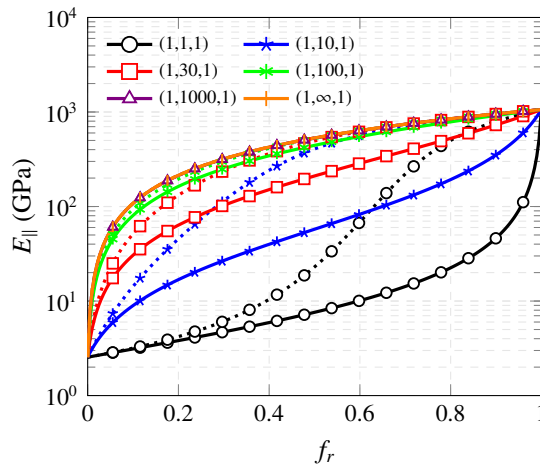


Figure 5: Effective Young's modulus in the longitudinal direction E_{\parallel} versus filler volume fraction f_r of Epon 862/EPI cure W reinforced by aligned, straight SWCNTs (10,10) with different aspect ratios, estimated by the MT and SC approaches, corresponding to solid and dotted lines, respectively.

Finally, Fig. 6 shows the elastic moduli of CNT/polymer composites considering the different chiralities from Table 2. It is noted that SWCNTs (5,5) and (50,50) yield the maximum and minimum moduli, respectively. To further this analysis, Fig. 7 investigates the elastic moduli as functions of the CNT radius. For armchair SWCNTs with chiral vector integers (n,n) , the radius of the CNTs can be computed as $r_{cnt} = 3nL_{cc}/2\pi$, being $L_{cc}=0.142$ nm the length of C-C bonds. It is observed in Fig. 7 that both E_{\parallel} and E_{\perp} substantially decrease with the CNT radius, as well as the degree of anisotropy. These results also explain the decreasing Young's moduli in Fig. 6 for increasing chiral vector integers (n,n) . In particular, SWCNTs (50,50) even reduce the transverse Young's modulus E_{\perp} . This chiral configuration corresponds to a tube radius of 0.339 \AA and has a transverse modulus of 0.4 GPa, below the Young's modulus of the polymer matrix. The surface contour of the Young's modulus of SWCNTs (50,50)/polymer is shown in Fig. 8 (a), and the planar projections on x_1 - x_2 plane are shown for different chiralities in Fig. 8 (b). It is stressed in this figure that lesser chiral integers, that is smaller filler diameters, dramatically increase the anisotropy of the composites.

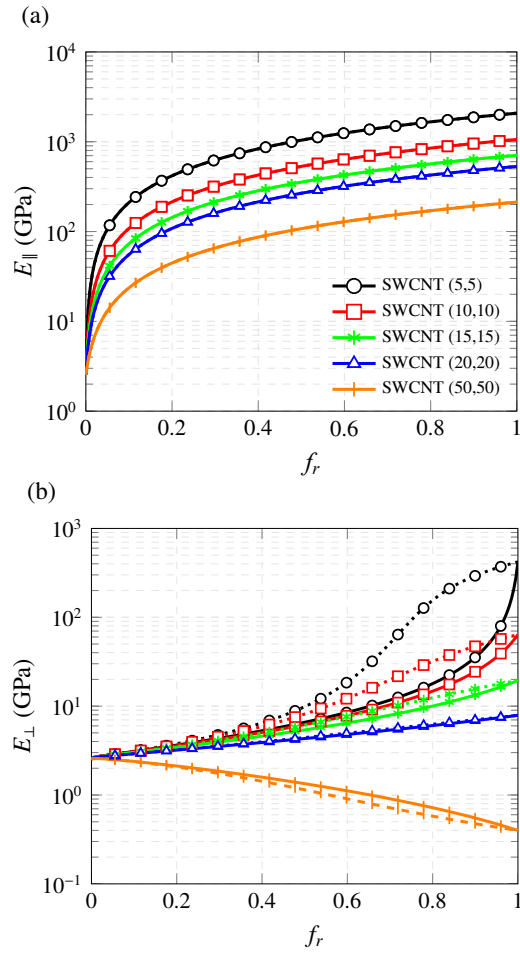


Figure 6: Effective Young's modulus in the longitudinal direction E_{\parallel} (a) and in the transverse direction E_{\perp} (b) versus filler volume fraction f_r of Epon 862/EPI reinforced by different aligned, straight SWCNTs (10,10), estimated by the MT and SC approaches, corresponding to solid and dotted lines, respectively.

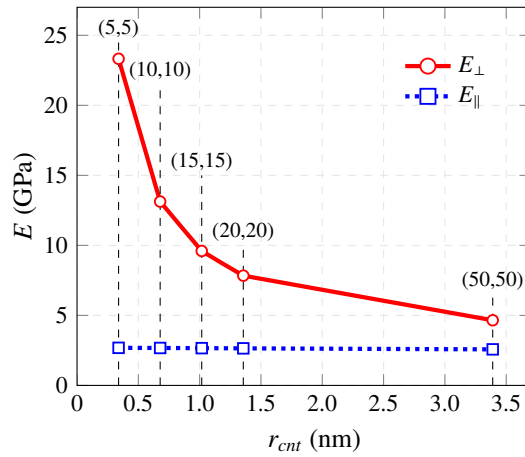


Figure 7: Longitudinal E_{\parallel} and transverse E_{\perp} Young's moduli of Epon 862/EPI reinforced by armchair SWCNTs versus CNT radius ($f_r=0.01$).

5.1.2. Misoriented CNTs

Let us move to the analysis of misoriented filler arrangements. In this work, the ODFs have been defined as truncated Gaussian distributions with azimuthal symmetry so that Ω is independent of γ . Hence, the ODF is

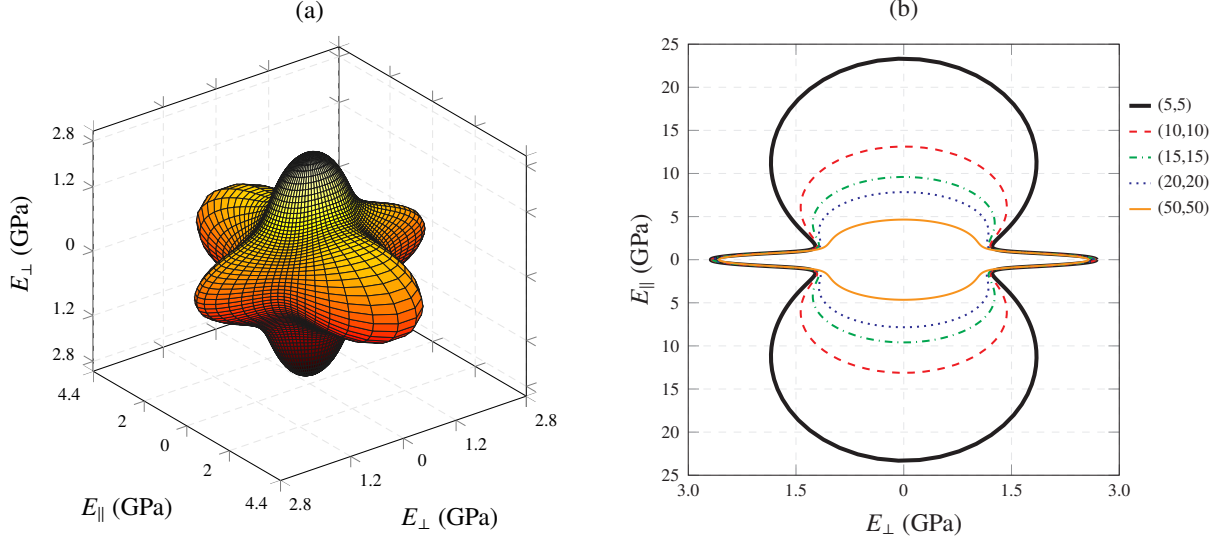


Figure 8: Surface contour of directional dependent Young's modulus ($f_r=0.01$, SWCNT (50,50)/Epon 862/EPI) (a) and planar projections on x_1-x_2 plane of Epon 862/EPI reinforced by armchair SWCNTs ($f_r=0.01$).

fully defined by a mean value $\mu = 0^\circ$ and a standard deviation σ . Fig. 9 furnishes the ODF for different standard deviations, namely $\sigma = 10^\circ, 30^\circ, 60^\circ$ and $\Omega(\theta) = 1/2\pi$, corresponding to a random filler arrangement.

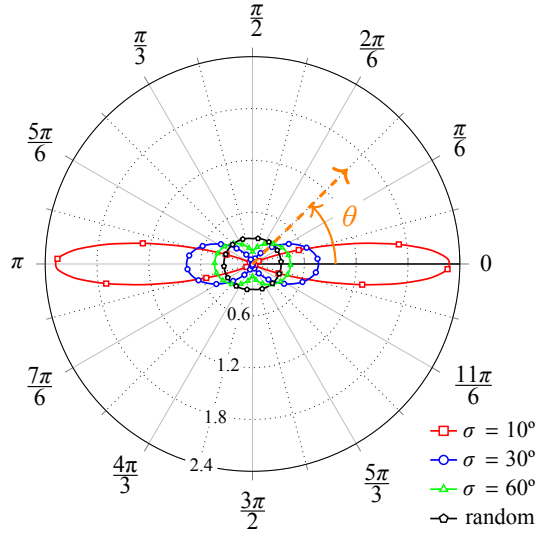


Figure 9: Polar plot of the symmetric truncated normal Orientation Distribution Function (ODF) $\Omega(\theta)$ for various standard deviations σ .

First, the estimates by the MT, SC, STP and DUN approaches are compared against theoretical bounds on elastic moduli for random filler arrangements ($\Omega(\theta) = 1/2\pi$). Fig. 10 shows the Young's modulus as a function of the filler volume fraction f_r . A first important conclusion is that the MT solution violates the HSW bound at a filler concentration around 67% and even exceeds the VT bound. This fact limits the applicability of the MT solution at high CNT volume fractions. With regard to the extended MT approaches, note that all the solutions converge to the VT bound at $f_r=1$. For validation purposes, the elastic modulus extracted by the orientational average $\langle C_r \rangle$, corresponding to the VT bound at $f_r=1$, has been computed using the closed-form solutions given by Zheng *et al.* [60]. The convergence of the numerical solutions demonstrates the correctness of the implemented approaches. The SC scheme also violates the upper HSW bound although it does lay within the VT/RS bounds. It is also observed that the DUN and STP approaches yield very close results and are comprised between the HSW bounds. With respect to the diagonal symmetry of the tensors, the estimates of the different approaches have been reported to be symmetric for random filler arrangements and, therefore, discussion in this regard is omitted. In quantitative terms, it is interesting to compare the different approaches when the MT approach coincides with the

U-HSW bound ($f_r = 0.67$). The MT and DE approaches yield elastic moduli of 268 GPa and 124 GPa. The SC predicts an elastic moduli between the two latter of value 213 GPa. Interestingly, the STP and DUN approaches provide very similar results with values around 129 GPa, half the one predicted by the MT approach.

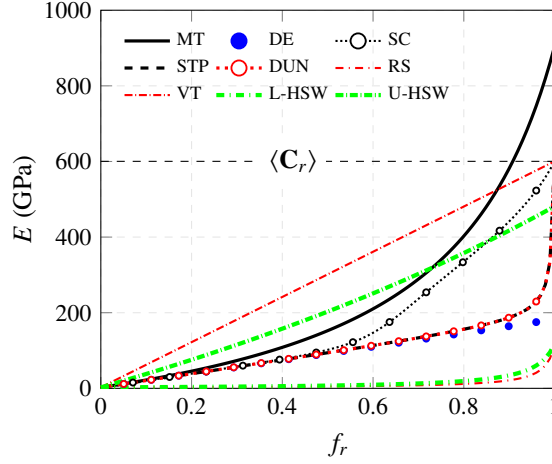


Figure 10: Young's modulus of Epon 862/EPI cure W reinforced by randomly oriented straight SWCNTs (10,10).

Finally, let us focus on misoriented CNT distributions. In this case, the diagonal symmetry of the estimates has to be verified. To this end, an asymmetry factor, AF_{ij} , can be defined as follows [25]:

$$AF_{ij} = 2 \frac{C(i, j) - C(j, i)}{C(i, j) + C(j, i)}, \quad i \neq j \quad (32)$$

being $C(i, j)$ the components of the stiffness tensor in Voigt notation. Fig. 11 shows the asymmetry factor of the MT estimates versus the orientation standard deviation σ for various filler contents. It can be observed that all the curves start at zero, as expected for fully aligned CNTs ($\sigma = 0^\circ$). In addition, the asymmetry factors also tend to zero for high standard deviation values until the limit case of random filler arrangements ($\Omega(\theta) = 1/2\pi$). It is noted that the asymmetry factors increase with the filler content, reaching maximum values around $\sigma = 10^\circ$. Despite the fact that the asymmetry factors are not excessively large, these estimates cannot be used in engineering applications since the resulting constitutive tensors are not positive definite. Given that the predictions of the DUN and STP approaches always yield diagonally symmetric stiffness tensors, that is zero asymmetry factors for every σ , they have been excluded in this analysis.

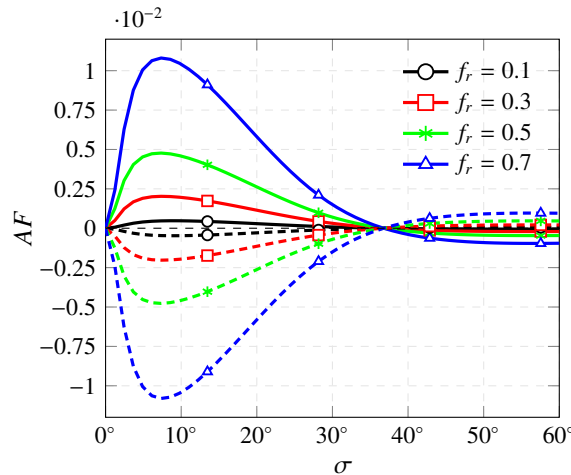


Figure 11: Asymmetry factor AF as a function of the orientation standard deviation σ for a symmetric truncated normal distribution obtained using the MT approach with different SWCNT (5,5) concentrations. Solid and dashed lines stand for AF_{12} and AF_{23} , respectively.

Finally, the effect of filler misalignment on the overall stiffness of CNT-reinforced composites is investigated. As previously discussed, the DUN and STP approaches yield similar results and, therefore, only the estimates

given by the STP approach are shown for clarity in the results. Given the azimuthal symmetry of the ODFs, the composites are transversely isotropic with x_1 - x_3 as the plane of isotropy. Fig. 12 depicts E_{\parallel} as a function of the CNT volume fraction with different degrees of filler misalignment. For illustrative purposes, SWCNTs (5,5) are selected as reinforcing phase. In this figure, it is clearly observed that variations of the misalignment degree induce considerable effects on the macroscopic Young's moduli. Also, it is noted that E_{\parallel} is bounded by that obtained for fully aligned ($\sigma = 0^\circ$) and randomly oriented CNTs ($\Omega(\theta) = 1/2\pi$). Further, Fig. 13 investigates the variation of E_{\parallel} and E_{\perp} as functions of σ . It is extracted from this analysis that the anisotropy of the composites decreases with increasing degrees of filler alignment. In the limit $\sigma \rightarrow \infty$, i.e. randomly oriented fillers, CNT/polymer composites are isotropic, $E_{\parallel} = E_{\perp}$.

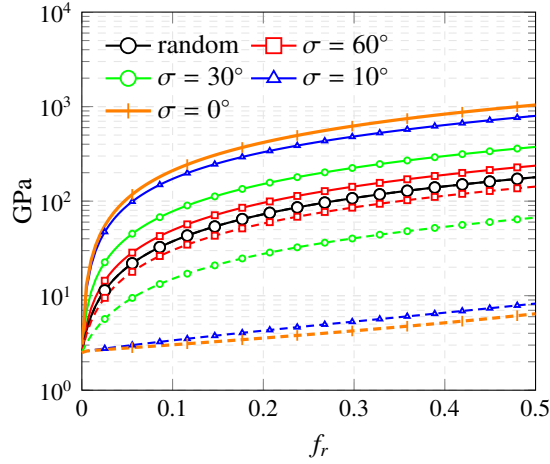


Figure 12: Elastic moduli as a function of volume fraction with different degrees of nanotube misalignment, for Epon 862/EPI reinforced by SWCNTs (5,5). Solid and dashed lines stand for longitudinal E_{\parallel} and transverse E_{\perp} Young's moduli.

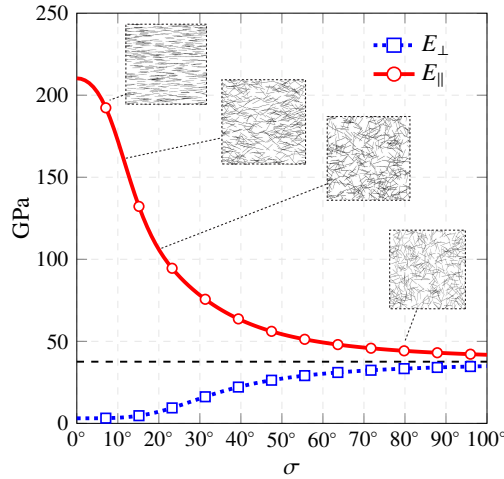


Figure 13: Longitudinal E_{\parallel} and transverse E_{\perp} Young's moduli as a function of orientation standard deviation σ of SWCNTs (5,5) with azimuthal symmetry ($f_r=0.1$).

5.2. Effect of CNT waviness

In this subsection, the effect of CNT waviness is investigated by the MT, YNS, and STP approaches. First, the diagonal symmetry condition must be verified. The direct integrations of the stiffness tensors appearing in both the YNS and STP approaches ensure that this condition is fulfilled. Nonetheless, this is not the case for the MT estimates. Figs. 14 (a) and (b) depict the asymmetry factors (AF_{12} and AF_{23}) as functions of the spiral angle θ^w and various filler volume fractions with fully aligned and helical SWCNTs (6,6)/(50,50) as reinforcing fillers, respectively. In both cases, the MT estimates are highly asymmetric, particularly for spiral angles $\theta^w = 0^\circ$, corresponding to circular fillers. As expected, the asymmetry condition is fulfilled ($AF_{ij} = 0$) for straight fillers, i.e. $\theta^w = 90^\circ$. Interestingly, it is noted that SWCNTs (50,50) lead to larger asymmetry factors, whereby it is

extracted that lesser anisotropic fillers yield more asymmetric estimates in Eq. (25). These results demonstrate that the MT approach cannot be directly applied to model CNT-reinforced composites with waviness effects and it is thereupon disregarded.

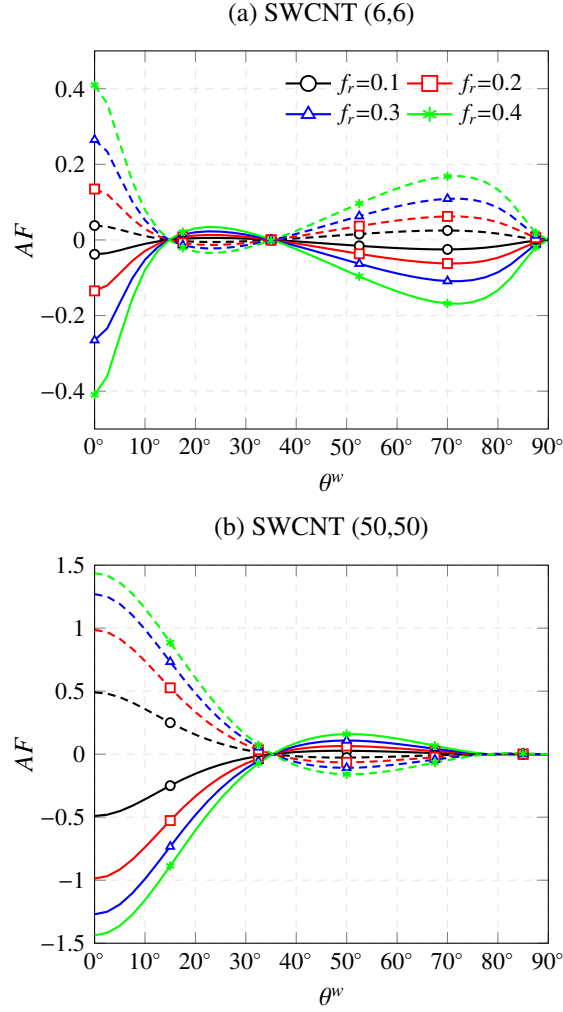


Figure 14: Asymmetry factors AF_{ij} as functions of the spiral angle θ^w for helical CNT-reinforced Epon 862/EPI obtained using the MT approach with different SWCNT (6,6) (a) and SWCNT (50,50) (b) concentrations. Solid and dashed lines stand for AF_{12} and AF_{23} , respectively.

Fig. 15 shows the elastic moduli of composites doped with fully aligned wavy SWCNTs (5,5) computed by the YNS and STP approaches. A volume fraction $f_r = 0.01$ is selected, and helical and planar sinusoidal configurations are depicted by solid and dashed lines, respectively. In order to compare both geometries, a waviness parameter is designated as A/λ . E_{22} stands for the macroscopic longitudinal Young's modulus, E_{11} and E_{33} are the transverse Young's moduli, and G_{12} denotes the longitudinal shear modulus of the composite. It is first observed that composites are orthotropic for planar sinusoidal geometries and transversely isotropic for the helical ones. Also, it is noted that the longitudinal Young's modulus E_{22} rapidly decreases as the waviness increases. With helical configurations, more pronounced reductions are found in E_{22} , while the transverse moduli $E_{11} = E_{33}$ slightly increase with the CNT waviness. For planar sinusoidal configurations, on the other hand, E_{33} substantially increases being the fillers defined on the x_2 - x_3 plane, whilst E_{11} remains approximately constant. With regard to the different homogenization approaches, it can be seen that the YNS approach provides slightly stiffer estimates. For instance, in the case of E_{11} and helical wavy fillers, maximum differences of 2% between the YNS and STP approaches are found for helical angles around $\theta^w = 61^\circ$. In the other two elastic moduli, even smaller differences are observed. In the case of planar sinusoidal geometries, maximum differences up to 6% are found for E_{22} and E_{33} for waviness parameters above $A/\lambda=0.15$. Finally, the highest differences between the STP and YNS approaches are noted for the shear modulus G_{12} , with maximum differences of 8% in the case of helical geometries.

Finally, the estimates for randomly distributed wavy CNTs are furnished in Fig. 16. In this case, the composites are isotropic and all the approaches provide diagonally symmetric estimates. It is first noted that the MT and

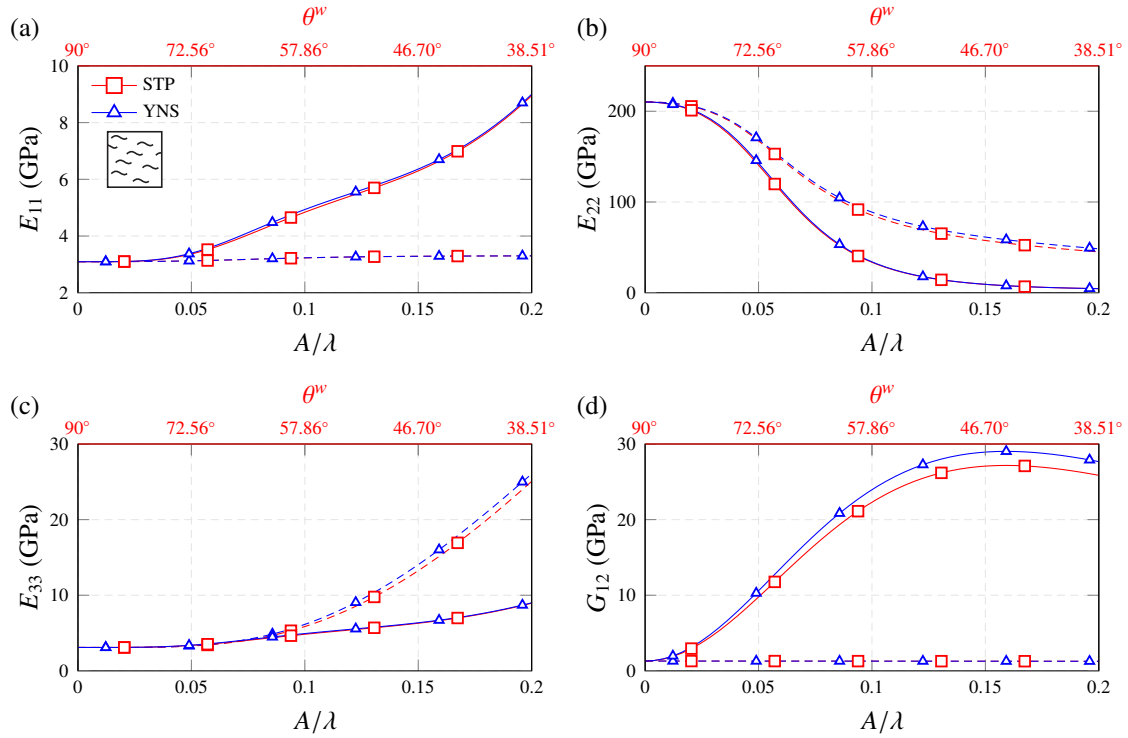


Figure 15: Elastic moduli predicted for Epon 862/EPI reinforced by fully aligned wavy SWCNTs (5,5) ($f_r=0.1$). Solid and dashed lines denote helical and planar sinusoidal configurations, respectively.

STP approaches yield predictions that are insensitive to waviness, unlike the YNS approach. This behavior is explained by the hypothesis of wavy fillers as consecutive infinitely long fibers in both the MT and STP approaches. Conversely, the YNS approach considers an ad hoc Eshelby's tensor, what results in a modified definition of the microstructure of the composite. In this case, decreasing Young's moduli are found for larger waviness parameters for both helical and planar sinusoidal configurations, with more acute reductions in the latter. Specifically, in the case of $A/\lambda = 0.4$ and helical filler configuration, the YNS approach provides an estimate of 38.75 GPa, 3% and 5% higher and lower than those provided by the STP and MT approaches, respectively.

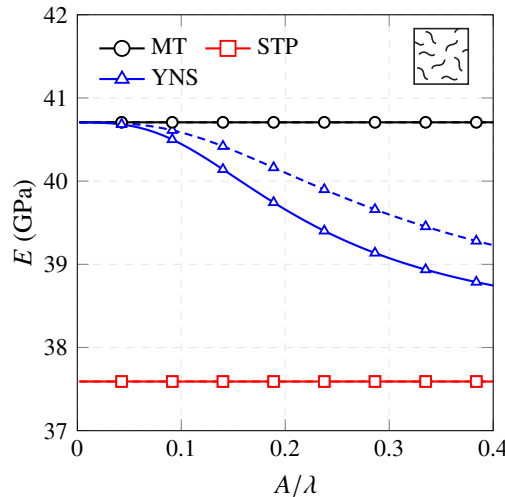


Figure 16: Elastic moduli predicted for Epon 862/EPI reinforced by randomly oriented wavy SWCNTs (5,5) ($f_r=0.1$). Solid and dashed lines denote helical and planar sinusoidal configurations, respectively.

5.3. Effect of CNT agglomeration

The effect of CNT agglomeration is studied on the basis of the two-parameter agglomeration framework. For randomly oriented CNTs with spherical bundles, Fig. 17 shows the variations of the overall Young's modulus with

respect to the agglomeration parameter ζ , while parameter ξ is kept constant at a value of 0.2. The effective properties have been estimated by the MT and STP approaches, corresponding to dashed and solid lines, respectively. It can be seen that, with the increase of ζ or, in other words, a larger number of CNTs agglomerated in bundles, the macroscopic elastic modulus experiences substantial decreases, especially for higher filler concentrations. Moreover, it is noted that the MT approach provides stiffer results, what finds the same explanation as in the previous analyses. In the particular case of $f_r=0.2$ and the STP approach, a reduction of 95% in the macroscopic elastic modulus is found when $\zeta=1$.

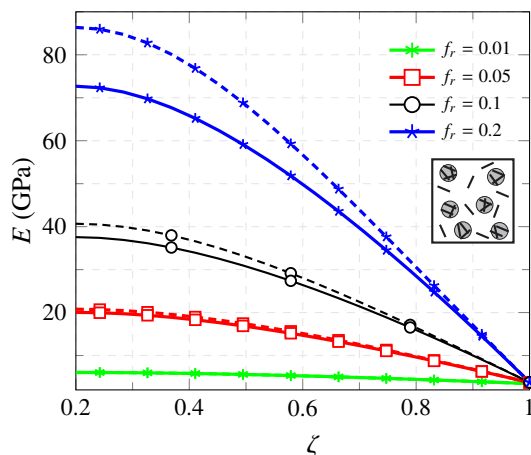


Figure 17: Macroscopic Young's modulus of Epon 862/EPI reinforced by randomly oriented SWCNTs (5,5) with agglomeration parameter $\xi=0.2$ and varying agglomeration parameter ζ . Dashed and solid lines denote estimations by the MT and SPT approaches, respectively.

For uniaxially aligned filler arrangements and spherical bundles, composites are transversely isotropic. Fig. 18 depicts E_{\parallel} and E_{\perp} as functions of the agglomeration parameter ζ . In this case, ξ is also kept constant at a value of 0.2. It is noted that agglomeration induces more severe weakening effects in the case of E_{\parallel} . Conversely, agglomeration of CNTs has little effect on E_{\perp} , which can even experience slight increases at high filler concentrations.

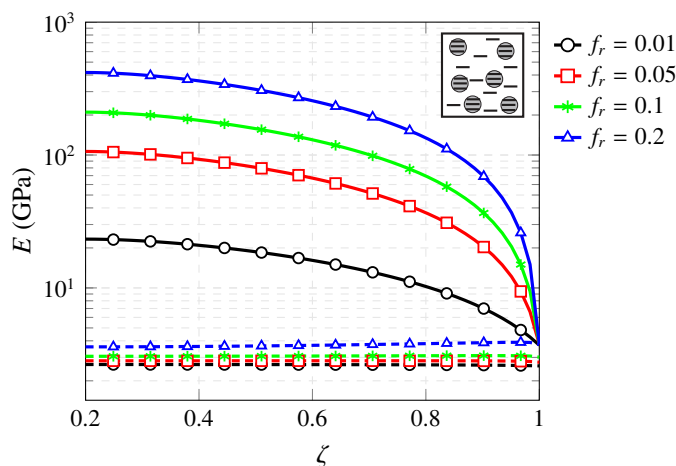


Figure 18: Macroscopic Young's modulus of Epon 862/EPI reinforced by fully aligned SWCNTs (5,5) with agglomeration parameter $\xi=0.2$ and varying agglomeration parameter ζ . Solid and dashed lines denote longitudinal E_{\parallel} and transverse elastic moduli E_{\perp} , respectively.

Finally, the effect of the aspect ratio of agglomerates is also studied by the STP approach in Fig. 19. In this figure, the stiffening efficiency (E/E_m and E_{\parallel}/E_m for randomly oriented and fully aligned CNTs, respectively) is plotted against the bundle aspect ratio a_2/a_1 . Let us recall that bundles are defined as ellipsoids of revolution with semi-axes $a_1=a_3 < a_2$. It is noted that the bundle aspect ratio exhibits moderate effects on the stiffening efficiency of polymers doped with randomly oriented CNTs. In addition, aspect ratios above 10 tend to an asymptotic value. On the contrary, the bundle aspect ratio has a deeper effect on the macroscopic properties of polymers doped with fully aligned CNTs. It is also observed in this case that the asymptotic value is reached at higher aspect

ratios. Overall, it is concluded that spherical bundles ($a_2/a_1=1$) infer the strongest weakening effects in both agglomeration schemes.

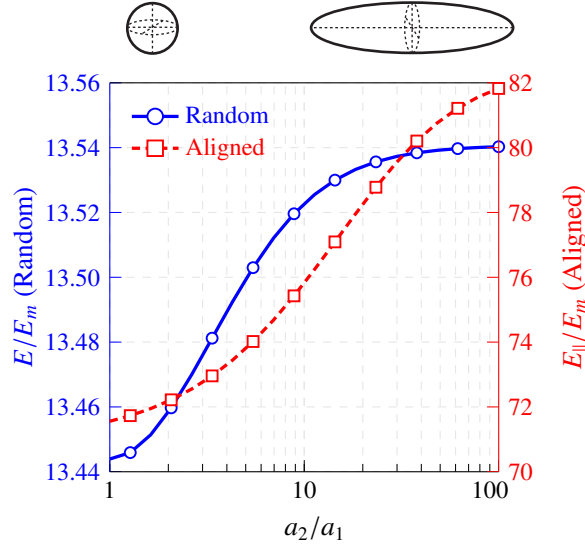


Figure 19: Effect of filler bundle aspect ratio (a_2/a_1) on the effective elastic properties of CNT-reinforced Epon 862/EPI Young's modulus of composites doped with randomly oriented CNTs, and longitudinal Young's modulus of composites doped with uniaxially aligned CNTs (SWCNT (5,5), $\xi=0.2$, $\zeta=0.4$, $f_r=0.1$).

5.4. Coupled effect of waviness and agglomeration

The coupled effect of waviness and agglomeration for randomly oriented CNT-reinforced polymers is investigated in Fig. 20. In this figure, the macroscopic Young's modulus is depicted against the helical spiral angle θ^w . The agglomeration parameter ξ is kept constant at a value of 0.2, and three different values of ζ are selected, namely $\zeta = 0.2, 0.3$ and 0.4 . Also, the global filler volume fraction is chosen as $f_r = 0.1$. Given that the MT approach for randomly oriented filler arrangements is insensitive to waviness as previously shown in Fig. 16, the YNS approach is combined with the two-parameter agglomeration model for this purpose. It is observed that the elastic modulus E decreases with higher agglomeration levels, that is to say, with larger ζ parameters. In addition, when waviness is also incorporated ($\theta^w < 90^\circ$), further reductions are found. For instance, in the case of $\xi = 0.2$ and $\zeta = 0.4$ and straight fillers, a reduction of 10.5% in the overall Young's modulus is found. However, when $\theta^w = 30^\circ$, the Young's modulus is further reduced up to 12.7%. Therefore, it is concluded that when both phenomena act simultaneously, their weakening effects add up.

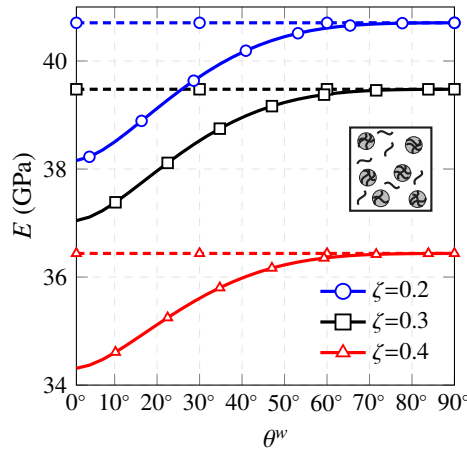


Figure 20: Macroscopic Young's modulus of Epon 862/EPI reinforced by randomly oriented wavy SWCNTs (5,5) with agglomeration parameter $\xi=0.2$ and varying agglomeration parameter ζ as a function of the spiral angle θ^w ($a_1=a_2=a_3$, $f_r=0.1$). Dashed lines denote the corresponding magnitudes for randomly oriented straight fillers.

5.5. Comparison against experimental data

In order to benchmark the studied approaches, a comparison analysis against experimental data is presented. In particular, the experimental results reported by Gao *et al.* [61] on the mechanical characterization of SWCNT-nylon 6 composites. In the simulations, SWCNTs (10,10) are selected and the elastic properties of the matrix are $E_m = 440$ MPa and $\nu_m = 0.2$ [61]. Since no especial aligning technique was reported in reference [61], SWCNTs are assumed to be randomly oriented. In normal practice, filler concentrations are typically provided in terms of mass fraction. The volume fraction of CNTs, f_r , can be calculated from the mass fraction, w_r , as:

$$f_r = \frac{w_r}{w_r + (\rho_r/\rho_m) - (\rho_r/\rho_m)w_r} \quad (33)$$

with ρ_r and ρ_m being the mass densities of CNT and matrix materials, respectively. Values of $\rho_r = 1.4$ g/cm³ [62] and $\rho_m = 1.184$ g/cm³ [61] are assumed in this work. Fig. 21 shows the comparison of the theoretical estimates provided by the MT, STP and DUN approaches along with the experimental data. Firstly, it is noted that all the approaches provide very similar estimates for such low filler contents. Despite the aforementioned deficiencies, this type of results highlights that the MT model remains important in practical applications, where CNT volume fractions are typically below 10%. Furthermore, it is observed that the theoretical simulations provide very close results to the experimental data until $w_r=0.2\%$, followed by considerable overestimations of the macroscopic elastic moduli. This is a fact that evidences the existence of agglomeration and/or waviness effects. Fig. 22 investigates the effects of filler agglomeration. Given that the used theoretical approaches provide very similar results, only the estimates by the STP model are shown for clarity. The agglomeration parameter ξ is kept constant at a value of 0.20, and five different values of ζ are selected, namely $\zeta=0.20, 0.50, 0.60, 0.75$ and 0.90 . It is noted that, in accordance with previous results, the agglomeration of fillers induces a considerable weakening effect on the macroscopic Young's modulus. In fact, the weakening effect increases with increasing filler contents in such a way that the good agreement between the theoretical and experimental data at low filler contents remains. It can be observed that an agglomeration parameter of $\zeta=0.60$ yields very close fittings with the experimental data up to $w_r=1.0\%$. After that, the homogenization approach overestimates the elastic modulus. It is interesting to note that the curve with agglomeration parameter $\zeta=0.9$ provides an estimate very close to the experimental result at $w_r=1.5\%$. This fact evidences the increasing tendency of CNTs with the filler content to form clusters. Hence, the agglomeration parameters should be considered as filler content dependent, a definition that is still missing in the literature. Finally, Fig. 23 furnishes the comparison of the theoretical estimates and the experimental data considering the coupled effect of waviness and agglomeration. To this aim, the two-parameter agglomeration model in combination with the YNS approach is utilized. On the basis of the previous results, the agglomeration parameters are selected as $\xi=0.2$ and $\zeta=0.6$, and five helical angles are considered, namely $\theta^w=10^\circ, 30^\circ, 50^\circ, 60^\circ$ and 90° . It is noted that the theoretical estimates get closer to the experimental data at filler contents of $w_r=1.0\%$ and 1.5% . However, there still exists a substantial overestimation of the macroscopic elastic modulus (≈ 0.4 GPa) at the filler content $w_r=1.5\%$, what evidences the existence of a higher level of filler agglomeration at this CNT concentration.

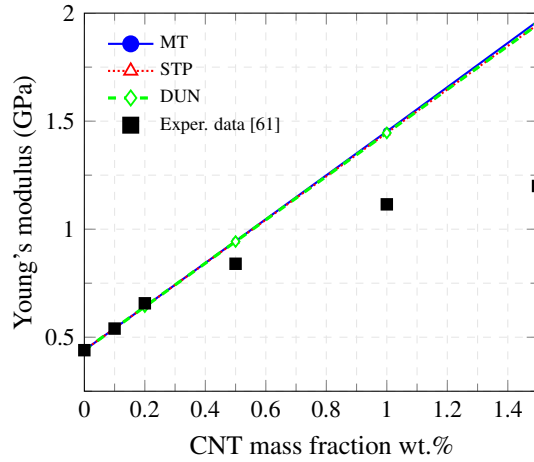


Figure 21: Comparison analysis of the macroscopic Young's modulus of SWCNT-nylon 6 composites considering randomly oriented straight uniformly dispersed fillers ($\rho_r=1.4$ g/cm³, $\rho_m=1.184$ g/cm³, SWCNTs (10,10), $E_m=440$ MPa, $\nu_m=0.2$).

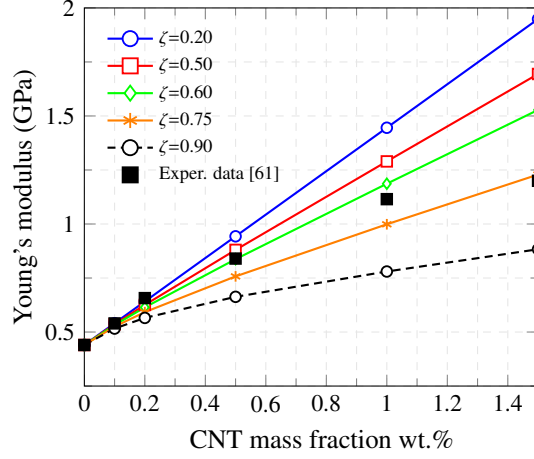


Figure 22: Comparison analysis of the macroscopic Young's modulus of SWCNT-nylon 6 composites considering randomly oriented straight dispersed fillers with agglomeration effects ($\rho_r=1.4 \text{ g/cm}^3$, $\rho_m=1.184 \text{ g/cm}^3$, SWCNTs (10,10), $E_m=440 \text{ MPa}$, $\nu_m=0.2$, $\xi=0.2$, $a_1=a_2=a_3$).

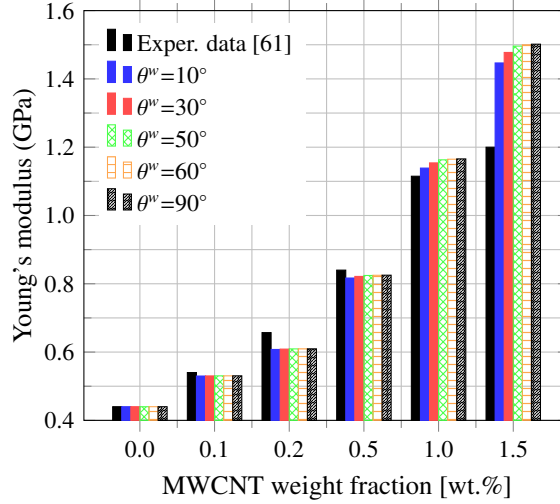


Figure 23: Comparison analysis of the macroscopic Young's modulus of SWCNT-nylon 6 composites considering randomly oriented helical fillers with agglomeration and waviness effects ($\rho_r=1.4 \text{ g/cm}^3$, $\rho_m=1.184 \text{ g/cm}^3$, SWCNTs (10,10), $E_m=440 \text{ MPa}$, $\nu_m=0.2$, $\xi=0.2$, $\zeta=0.6$, $a_1=a_2=a_3$).

5.6. Case study: vibrational analysis of CNT/polymer skew plates

Finally, the vibrational behavior of CNT/polymer skew plates is studied on the basis of the preceding discussions. To this aim, a finite element formulation based on the Hu-Washizu principle for skew shells developed by the authors in reference [63] is utilized. In that work, thin and moderately thick functionally graded skew plates doped with uniaxially aligned fillers were studied using the EROM. In these tests, only uniform filler gradings are studied for illustrative purposes, considering both waviness and agglomeration effects. Fig. 24 shows the geometrical configuration of the skew plates, with length a , width b , thickness t , filler orientation angle φ , and skew angle α . Simply supported boundary conditions are studied, and the mass densities of the matrix and reinforcing phases are selected as $\rho_m = 1.15 \text{ g/cm}^3$ and $\rho_m = 1.40 \text{ g/cm}^3$, respectively. Also, a global filler volume fraction $f_r = 0.12$ is selected, as well as SWCNTs (5,5) as reinforcing phase. The effective material properties of the composites are computed by the YNS approach in combination with the two-parameter agglomeration model. The resonant frequencies ω and the natural modes of vibration are computed by solving the eigenvalue problem associated to the undamped free vibration system. In the subsequent results, the computed resonant frequencies are all presented in non-dimensional form as follows:

$$\lambda = \omega \frac{b^2}{t} \sqrt{\frac{\rho_m}{E_m}} \quad (34)$$

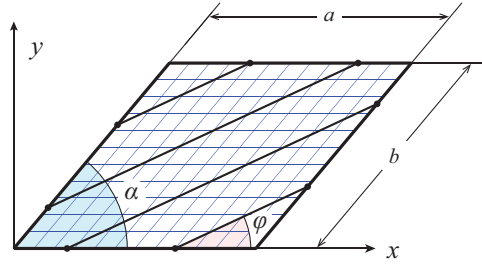


Figure 24: Geometry and configuration of CNT/polymer skew plates.

Firstly, skew plates doped with fully aligned filler arrangements are studied. Fig. 25 shows the variation of the fundamental frequency parameter, λ_1 , against the filler angle φ for several skew angles α . The skew plates are defined with a length-to-width ratio of $a/b = 1$, and a width-to-thickness ratio of $b/t = 50$. In accordance with previously published results in reference [63], it is noted that the CNT orientation critically determines the dynamic behavior of CNT-reinforced skew plates and, hence, plays a key role in their design. However, it is paramount to evaluate the effect of the filler waviness that may arise in the manufacturing process. To this end, Fig. 26 furnishes the results obtained for skew plates with $\alpha = 60^\circ$ and considering various degrees of helical waviness. It is observed that the CNT waviness substantially alters the dynamic properties of the plates. Overall, stiffer results are obtained for fillers aligned in the direction of the longest diagonal, while smaller values are found for fillers aligned in its transverse direction. Thence, the vibrational behavior of the plates is mainly determined by the material anisotropy, which is highly dependent on the degree of CNT curviness.

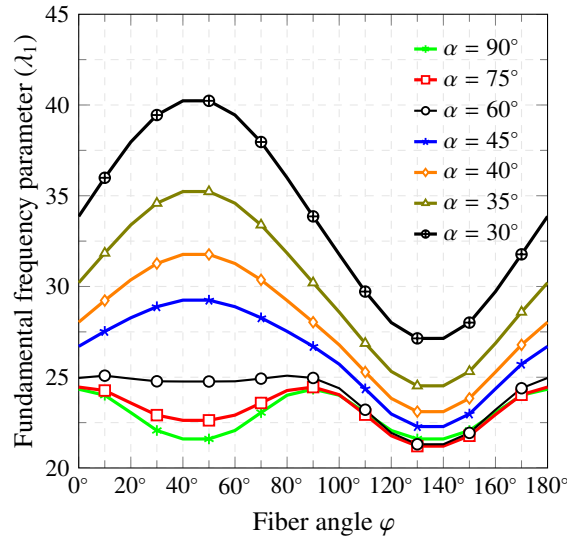


Figure 25: Effect of fiber angle φ on the first frequency parameter λ_1 of CNT/polymer skew plates ($f_r = 0.12$, $a/b = 1$, $b/t = 50$, SWCNT (5,5)).

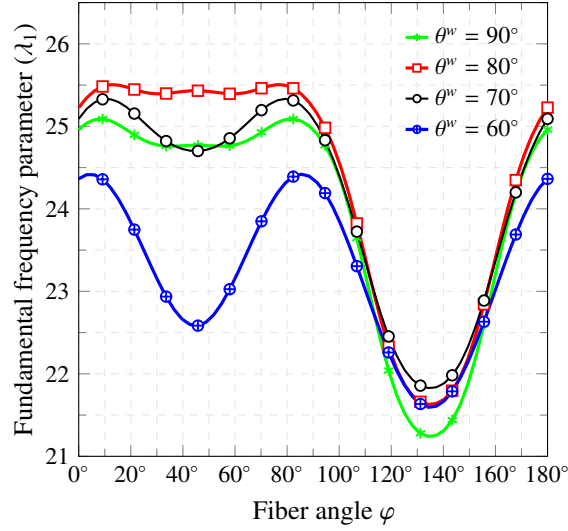


Figure 26: Effect of fiber angle φ on the first frequency parameter λ_1 of CNT/polymer skew plates with waviness effects ($\alpha = 60^\circ$, $f_r = 0.12$, $a/b = 1$, $b/t = 50$, SWCNT (5,5)).

The effect of CNT agglomeration on the vibrational behavior of CNT-reinforced skew plates with randomly filler arrangements is also evaluated. For this purpose, a harmonic analysis is performed to ascertain the corresponding amplitude (in dB) of the Frequency Response Function (FRF). The FRF of a driving point located at the center of the plates is shown in Fig. 27. For illustrative purposes, a constant modal damping ratio of 1% is assumed. Also, the agglomeration parameter ξ is kept constant at a value of 0.2, and three different values of ζ are selected, namely $\zeta = 0.2, 0.3, 0.4$ and 0.5 . It is noted that four mode shapes are comprised in the frequency range $\lambda \in [0, 110]$. In particular, the first peak in the spectrum corresponds to the first bending mode, the second and third peaks to second bending modes and, finally, the fourth peak to a third bending mode. As expected, filler agglomeration reduces the overall stiffness of the composites and, as a consequence, the peaks in the spectrum shift towards lesser frequencies, especially for high natural modes. Further, Fig. 28 examines the combined effect of waviness and agglomeration, as it is commonly the case in practical applications. For the sake of clarity, the FRF is limited to a frequency range surrounding the fundamental frequency. In this analysis, the agglomeration parameters are selected as $\xi=0.2$ and $\zeta=0.4$, and several spiral angles are selected, namely $\theta^w = 90^\circ, 80^\circ, 60^\circ$ and 50° . In accordance with the previous results, it is noted that CNT waviness renders further shifts of the peaks in the spectrum towards lower frequencies, that is more flexible structures, what stresses the importance of the combined weakening effects of filler waviness and agglomeration.

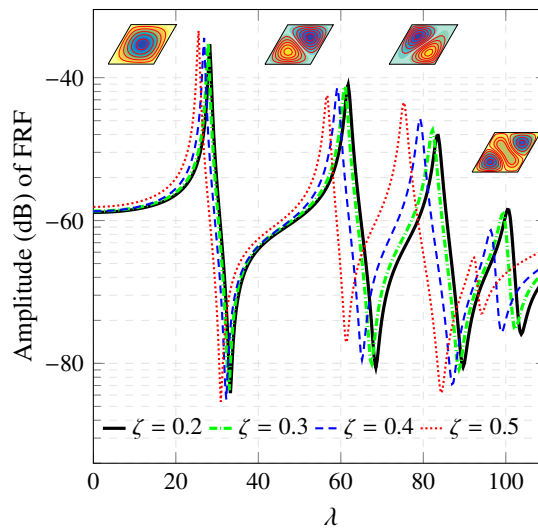


Figure 27: Frequency response function (FRF) plot of CNT/polymer skew plates with agglomeration effects ($f_r = 0.12$, $\xi=0.2$, $a/b = 1$, $b/t = 50$, SWCNT (5,5)).

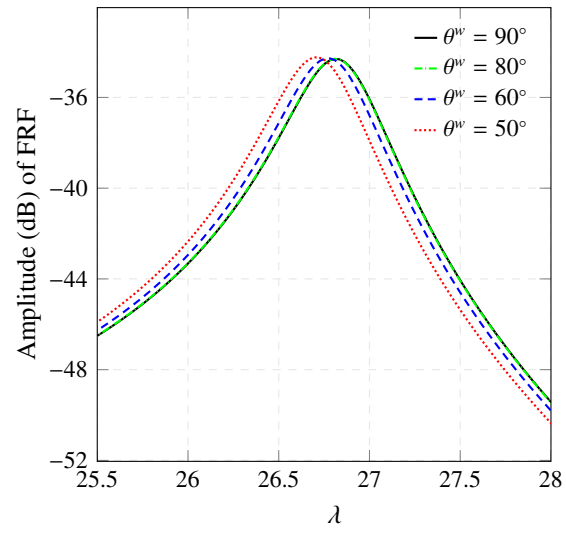


Figure 28: Frequency response function (FRF) plot of CNT/polymer skew plates with coupled waviness and agglomeration effects ($f_r = 0.12$, $\xi=0.2$, $\zeta=0.4$, $a/b = 1$, $b/t = 50$, SWCNT (5,5)).

6. Conclusions

This article has presented a critical comparison of different mean-field homogenization approaches for CNT-reinforced polymer composites with waviness and agglomeration effects. Firstly, the MT, SC, DUN and STP approaches have been compared in terms of diagonal symmetry and against the HSW and RS/VT bounds for misoriented CNT arrangements. Afterward, the MT, STP and YNS approaches have been analyzed for both planar sinusoidal and three-dimensional helical CNTs, including fully aligned and randomly oriented wavy filler arrangements. Through a two-parameter agglomeration framework, the influence of the filler agglomeration on the macroscopic stiffness of CNT-reinforced composites has been also investigated. The results have evidenced that the MT method fails to simulate the coupled effect of waviness and agglomeration, providing estimates that are insensitive to waviness for random filler arrangements. Furthermore, it has been shown that the MT predictions for composites doped with fully aligned wavy CNTs are highly asymmetric and, thus, physically inadmissible. By considering the combination of the YNS approach and the two-parameter agglomeration model, it has been shown that the weakening effects of waviness and agglomeration add up when acting simultaneously. Then, a comparison analysis against experimental data has highlighted the importance of considering agglomeration and waviness for moderate filler volume contents. Finally, a case study has been also presented, whereby it has been highlighted that filler waviness and agglomeration exhibit a coupled weakening effect on the macroscopic dynamic behavior of CNT-reinforced skew plates.

The key findings of this work can be summarized as follows:

- In the case of uniaxially aligned fillers, it has been shown that the SC and the MT approaches provide very close estimates of the longitudinal Young's modulus, while the SC model predicts transverse moduli that are four times the one obtained by the MT model at a filler content $f_v=0.8$. In the case of randomly oriented CNTs, it has been shown that the MT solution violates the HSW bounds at filler volume fractions above 67%, unlike the DUN and STP approaches which always provide estimates that are comprised between the HSW bounds. The results have also reported that the MT provides estimates 50% higher than those predicted by the STP and DUN approaches for moderate filler contents. Nevertheless, these differences get reduced for low filler volume fractions as typically found in normal practice, a fact that advocates the practical importance of the MT approach.
- In the case of fully aligned wavy CNTs, the MT approach has been reported to provide highly asymmetric stiffness tensors and, thus, physically inadmissible estimates. Also, the numerical results have shown very close agreements between the STP and YNS approaches, with slightly stiffer predictions in the latter, and maximum differences of 6% and 8% in the estimated Young's and shear moduli, respectively.
- Filler agglomeration has been proven to induce detrimental effects on the mechanical properties for both randomly oriented and fully aligned CNTs, with more severe effects in the latter.
- The results have evidenced that filler waviness and agglomeration have coupled weakening effects when acting together. It has been shown that only the YNS approach in combination with the two-parameter agglomeration model can properly account for both phenomena simultaneously. The reason for this behavior is ascribed to the ad hoc definition of the Eshelby's tensor that accounts for the particular wavy geometry of the fillers.
- The comparison against experimental data has evidenced the importance of CNT agglomeration and waviness effects. The assumption of ideal conditions of uniformly distributed straight fillers has been shown to lead to severe overestimations of the elastic modulus of CNT-reinforced composites for moderate filler contents. The application of the two-parameter agglomeration model and the STP approach has yielded close agreements with the experimental data. Also, the application of the YNS approach to account for the coupled effect of waviness and agglomeration has been shown to provide closer fittings for moderate CNT contents.
- A case study on the vibrational properties of CNT-reinforced skew plates has been presented. The results have demonstrated that CNT waviness and agglomeration exhibit additive weakening effects on the macroscopic response of full-scale composite structures.

Acknowledgement

This work was supported by the Ministerio de Economía y Competitividad of Spain under the project DPI2014-53947-R. E. G-M was also supported by a FPU contract-fellowship from the Spanish Ministry of Education Ref: FPU13/04892. The financial support is gratefully acknowledged.

References

- [1] J. N. Coleman, U. Khan, W. J. Blau, Y. K. Gunko, Small but strong: a review of the mechanical properties of carbon nanotube–polymer composites, *Carbon* 44 (2006) 1624–1652.
- [2] Z. Spitalsky, D. Tasis, K. Papagelis, C. Galiotis, Carbon nanotube–polymer composites: Chemistry, processing, mechanical and electrical properties, *Progress in Polymer Science* 35 (2010) 357–401.
- [3] W. Salalha, Y. Dror, R. L. Khalfin, Y. Cohen, A. L. Yarin, E. Zussman, Single-walled carbon nanotubes embedded in oriented polymeric nanofibers by electrospinning, *Langmuir* 20 (2004) 9852–9855.
- [4] M. S. Al-Haik, H. Garmestani, D. S. Li, M. Y. Hussaini, S. S. Sablin, R. Tannenbaum, K. Dahmen, Mechanical properties of magnetically oriented epoxy, *Journal of Polymer Science Part B: Polymer Physics* 42 (2004) 1586–1600.
- [5] C. A. Mitchell, J. L. Bahr, S. Arepalli, J. M. Tour, R. Krishnamoorti, Dispersion of functionalized carbon nanotubes in polystyrene, *Macromolecules* 35 (2002) 8825–8830.
- [6] E. Camponeschi, R. Vance, M. Al-Haik, H. Garmestani, R. Tannenbaum, Properties of carbon nanotube–polymer composites aligned in a magnetic field, *Carbon* 45 (2007) 2037–2046.
- [7] B. Vigolo, Macroscopic fibers and ribbons of oriented carbon nanotubes, *Science* 290 (2000) 1331–1334.
- [8] R. H. Poelma, X. Fan, Z. Y. Hu, G. Van Tendeloo, H. W. van Zeijl, G. Q. Zhang, Effects of nanostructure and coating on the mechanics of carbon nanotube arrays, *Advanced Functional Materials* 26 (2016) 1233–1242.
- [9] A. Allaoui, S. Bai, H. Cheng, J. Bai, Mechanical and electrical properties of a MWNT/epoxy composite, *Composites Science and Technology* 62 (2002) 1993–1998.
- [10] H. Li, H. Xiao, J. Yuan, J. Ou, Microstructure of cement mortar with nano-particles, *Composites Part B: Engineering* 35 (2004) 185–189.
- [11] J. M. Wernik, S. A. Meguid, Recent developments in multifunctional nanocomposites using carbon nanotubes, *Applied Mechanics Reviews* 63 (2010) 050801.
- [12] M. Griebel, J. Hamaekers, Molecular dynamics simulations of the elastic moduli of polymer–carbon nanotube composites, *Computer Methods in Applied Mechanics and Engineering* 193 (2004) 1773–1788.
- [13] R. Zhu, E. Pan, A. Roy, Molecular dynamics study of the stress–strain behavior of carbon-nanotube reinforced Epon 862 composites, *Materials Science and Engineering: A* 447 (2007) 51–57.
- [14] M. M. Shokrieh, R. Rafiee, Prediction of mechanical properties of an embedded carbon nanotube in polymer matrix based on developing an equivalent long fiber, *Mechanics Research Communications* 37 (2010) 235–240.
- [15] A. Alian, S. El-Borgi, S. Meguid, Multiscale modeling of the effect of waviness and agglomeration of CNTs on the elastic properties of nanocomposites, *Computational Materials Science* 117 (2016) 195–204.
- [16] H. S. Shen, Y. Xiang, Postbuckling of pressure-loaded nanotube-reinforced composite doubly curved panels resting on elastic foundations in thermal environments, *International Journal of Mechanical Sciences* 107 (2016) 225–234.
- [17] Q. Wang, X. Cui, B. Qin, Q. Liang, Vibration analysis of the functionally graded carbon nanotube reinforced composite shallow shells with arbitrary boundary conditions, *Composite Structures* 182 (2017) 364–379.
- [18] Y. Kiani, Thermal post-buckling of FG-CNT reinforced composite plates, *Composite Structures* 159 (2017) 299–306.
- [19] F. Tornabene, N. Fantuzzi, M. Baccocchi, E. Viola, Effect of agglomeration on the natural frequencies of functionally graded carbon nanotube-reinforced laminated composite doubly-curved shells, *Composites Part B: Engineering* 89 (2016) 187–218.
- [20] E. García-Macías, L. Rodríguez-Tembleque, R. Castro-Triguero, A. Sáez, Buckling analysis of functionally graded carbon nanotube-reinforced curved panels under axial compression and shear, *Composites Part B: Engineering* 108 (2017) 243–256.

- [21] K. Mehar, S. K. Panda, T. R. Mahapatra, Theoretical and experimental investigation of vibration characteristic of carbon nanotube reinforced polymer composite structure, *International Journal of Mechanical Sciences* 133 (2017) 319–329.
- [22] H. Shen, Nonlinear bending of functionally graded carbon nanotube-reinforced composite plates in thermal environments, *Composite Structures* 91 (2009) 9–19.
- [23] D. Shi, X. Feng, Y. Y. Huang, K. Hwang, H. Gao, The effect of nanotube waviness and agglomeration on the elastic property of carbon nanotube-reinforced composites, *Journal of Engineering Materials and Technology* 126 (2004) 250–257.
- [24] A. N. Norris, An examination of the Mori-Tanaka effective medium approximation for multiphase composites, *Journal of Applied Mechanics* 56 (1989) 83.
- [25] Y. Qiu, G. Weng, On the application of Mori-Tanaka's theory involving transversely isotropic spheroidal inclusions, *International Journal of Engineering Science* 28 (1990) 1121–1137.
- [26] M. Ferrari, Asymmetry and the high concentration limit of the Mori-Tanaka effective medium theory, *Mechanics of Materials* 11 (1991) 251–256.
- [27] Y. Benveniste, G. Dvorak, T. Chen, On diagonal and elastic symmetry of the approximate effective stiffness tensor of heterogeneous media, *Journal of the Mechanics and Physics of Solids* 39 (1991) 927–946.
- [28] M. Ferrari, Composite homogenization via the equivalent poly-inclusion approach, *Composites Engineering* 4 (1994) 37–45.
- [29] M. L. Dunn, H. Ledbetter, P. R. Heyliger, C. S. Choi, Elastic constants of textured short-fiber composites, *Journal of the Mechanics and Physics of Solids* 44 (1996) 1509–1541.
- [30] J. Schjødt-Thomsen, R. Pyrz, The Mori-Tanaka stiffness tensor: diagonal symmetry, complex fibre orientations and non-dilute volume fractions, *Mechanics of Materials* 33 (2001) 531–544.
- [31] O. I. Zhupanska, The effect of orientational distribution of nanotubes on buckypaper nanocomposite mechanical properties, *Mechanics of Advanced Materials and Structures* 20 (2013) 1–10.
- [32] F. Fisher, R. Bradshaw, L. Brinson, Fiber waviness in nanotube-reinforced polymer composites–I: Modulus predictions using effective nanotube properties, *Composites Science and Technology* 63 (2003) 1689–1703.
- [33] R. D. Bradshaw, F. T. Fisher, L. C. Brinson, Fiber waviness in nanotube-reinforced polymer composites–II: modeling via numerical approximation of the dilute strain concentration tensor, *Composites Science and Technology* 63 (2003) 1705–1722.
- [34] H. Hsiao, I. Daniel, Elastic properties of composites with fiber waviness, *Composites Part A: Applied Science and Manufacturing* 27 (1996) 931–941.
- [35] K. Yanase, S. Moriyama, J. W. Ju, Effects of CNT waviness on the effective elastic responses of CNT-reinforced polymer composites, *Acta Mechanica* 224 (2013) 1351–1364.
- [36] A. Y. Matveeva, S. V. Pyrlin, M. M. Ramos, H. J. Böhm, F. W. van Hattum, Influence of waviness and curliness of fibres on mechanical properties of composites, *Computational Materials Science* 87 (2014) 1–11.
- [37] B. S. Aragh, A. N. Barati, H. Hedayati, Eshelby-Mori-Tanaka approach for vibrational behavior of continuously graded carbon nanotube-reinforced cylindrical panels, *Composites Part B: Engineering* 43 (2012) 1943–1954.
- [38] F. Tornabene, N. Fantuzzi, M. Baccocchi, Linear static response of nanocomposite plates and shells reinforced by agglomerated carbon nanotubes, *Composites Part B: Engineering* 115 (2017) 449–476.
- [39] M. Nejati, A. Asanjarani, R. Dimitri, F. Tornabene, Static and free vibration analysis of functionally graded conical shells reinforced by carbon nanotubes, *International Journal of Mechanical Sciences* 130 (2017) 383–398.
- [40] S. Kamarian, M. Salim, R. Dimitri, F. Tornabene, Free vibration analysis of conical shells reinforced with agglomerated carbon nanotubes, *International Journal of Mechanical Sciences* 108 (2016) 157–165.

- [41] S. Nemat-Nasser, M. Hori, *Micromechanics: overall properties of heterogeneous materials*, volume 37, Elsevier, 2013.
- [42] R. Hill, A self-consistent mechanics of composite materials, *Journal of the Mechanics and Physics of Solids* 13 (1965) 213–222.
- [43] L. Walpole, On the overall elastic moduli of composite materials, *Journal of the Mechanics and Physics of Solids* 17 (1969) 235–251.
- [44] T. Mori, K. Tanaka, Average stress in matrix and average elastic energy of materials with misfitting inclusions, *Acta metallurgica* 21 (1973) 571–574.
- [45] J. D. Eshelby, The determination of the elastic field of an ellipsoidal inclusion, and related problems, *Proceedings of the Royal Society of London. Series A. Mathematical and Physical Sciences* 241 (1957) 376–396.
- [46] J. Eshelby, The elastic field outside an ellipsoidal inclusion, *Proceedings of the Royal Society of London. Series A, Mathematical and Physical Sciences* (1959) 561–569.
- [47] T. Mura, *Micromechanics of defects in solids*, volume 3, Springer Science & Business Media, 1987.
- [48] Y. Benveniste, A new approach to the application of Mori-Tanaka’s theory in composite materials, *Mechanics of materials* 6 (1987) 147–157.
- [49] T. W. Chou, S. Nomura, M. Taya, A self-consistent approach to the elastic stiffness of short-fiber composites, *Journal of Composite Materials* 14 (1980) 178–188.
- [50] S. C. Lin, T. Mura, Elastic fields of inclusions in anisotropic media (II), *Physica Status Solidi (a)* 15 (1973) 281–285.
- [51] E. García-Macías, A. D’Alessandro, R. Castro-Triguero, D. Pérez-Mira, F. Ubertini, Micromechanics modeling of the uniaxial strain-sensing property of carbon nanotube cement-matrix composites for SHM applications, *Composite Structures* 163 (2017) 195–215.
- [52] W. S. Bao, S. A. Meguid, Z. H. Zhu, Y. Pan, G. J. Weng, Effect of carbon nanotube geometry upon tunneling assisted electrical network in nanocomposites, *Journal of Applied Physics* 113 (2013) 234313.
- [53] F. Tornabene, M. Baccocchi, N. Fantuzzi, J. N. Reddy, Multiscale approach for three-phase CNT/polymer/fiber laminated nanocomposite structures, *Polymer Composites* (2017).
- [54] L. Shen, J. Li, Transversely isotropic elastic properties of single-walled carbon nanotubes, *Physical Review B* 69 (2004).
- [55] W. Voigt, Ueber die beziehung zwischen den beiden elasticitätsconstanten isotroper krper, *Annalen der Physik* 274 (1889) 573–587.
- [56] A. Reuss, Calculation of the flow limits of mixed crystals on the basis of the plasticity of monocrystals, *Z. Angew. Math. Mech* 9 (1929) 49–58.
- [57] Z. Hashin, S. Shtrikman, On some variational principles in anisotropic and nonhomogeneous elasticity, *Journal of the Mechanics and Physics of Solids* 10 (1962) 335–342.
- [58] Z. Hashin, S. Shtrikman, A variational approach to the theory of the elastic behaviour of multiphase materials, *Journal of the Mechanics and Physics of Solids* 11 (1963) 127–140.
- [59] L. Walpole, On bounds for the overall elastic moduli of inhomogeneous systems—I, *Journal of the Mechanics and Physics of Solids* 14 (1966) 151–162.
- [60] X. Zheng, M. G. Forest, R. Lipton, R. Zhou, Nematic polymer mechanics: flow-induced anisotropy, *Continuum Mechanics and Thermodynamics* 18 (2006) 377–394.
- [61] J. Gao, M. E. Itkis, A. Yu, E. Bekyarova, B. Zhao, R. C. Haddon, Continuous spinning of a single-walled carbon nanotube-nylon composite fiber, *Journal of the American Chemical Society* 127 (2005) 3847–3854.
- [62] H. S. Shen, Y. Xiang, Nonlinear vibration of nanotube-reinforced composite cylindrical panels resting on elastic foundations in thermal environments, *Composite Structures* 111 (2014) 291–300.

- [63] E. García-Macías, R. Castro-Triguero, E. I. S. Flores, M. I. Friswell, R. Gallego, Static and free vibration analysis of functionally graded carbon nanotube reinforced skew plates, *Composite Structures* 140 (2016) 473–490.